Improving a six-wheeler's performance both on- and off-road

Olof Noréus

Doctoral Thesis

TRITA-AVE 2010:61
ISSN 1651-7660
ISBN 978-91-7415-766-6

Postal address	**Visiting address**	**Telephone**	**Internet**
Royal Institute of Technology	Teknikringen 8	+46 8 790 6000	www.ave.kth.se
Vehicle Dynamics	Stockholm	**Telefax**	
SE-100 44 Stockholm		+46 0 790 9290	

Typeset using LaTeX with LyX frontend

Abstract

In vehicles with electric transmission and independent wheel stations, there is a possibility to control propulsion, steering and suspension individually for each wheel. This makes it possible to improve mobility in terrain as well as performance and driving safety on road. This contribution concerns how a six wheeled electric transmission vehicle should be modelled to enable evaluation of the dynamic behaviour both in terrain and on road. This is made by combining modelling of vehicle, transmission and tyre/terrain behaviour.

A tyre/terrain model is needed to simulate driving on soft ground. Here tyre/terrain models for simulating driving with both rigid and pneumatic wheels on soft ground have been developed. A method to measure terrain parameters and drawbar pull for a six-wheeled vehicle on sand is proposed, tested and evaluated.

To simulate a six wheeled vehicle at the handling limit on road, a vehicle model with a brush tyre model is used in order to get physically reasonable simulation results during high combined slip conditions. Different vehicle configurations are considered, where front wheel steering is combined with either second axle steering, rear wheel steering or individual wheel torque control. By applying different vehicle slip angles and thereby limiting the DOF of the vehicle model, the vehicle configurations are evaluated during different driving conditions. The results show that by applying individual torque control to the front wheel steered vehicle, the performance is improved for all evaluated manoeuvres, and the achievable aligning torque during a rear wheel skid increases significantly if the vehicle slip angle is larger than the maximum front wheel steering angle.

To conclude, models of a six-wheeled vehicle with electric transmission and tyre models both for soft and rigid ground have been developed. These models form a simulation platform, which makes it possible to evaluate control strategies for the electric transmission with the purpose to improve mobility in terrain as well as performance and driving safety on road. Some examples of applications of the models are included, e.g. improving at-the-limit handling and pivot turning performance.

Acknowledgements

The thesis work has been carried out within a part-time research project from year 2002 to 2010 at BAE Systems Hägglunds AB (Hägglunds) in Örnsköldsvik and the division of Vehicle Dynamics at the Royal Institute of Technology (KTH) in Stockholm, Sweden.

The project was financed by Hägglunds with the purpose to increase the mobility, understanding and take advantage of the control possibilities with electric transmissions in new vehicle concepts. The project has been Hägglunds contribution to the Gröna Bilen National Research Programme within the FCHEV framework between year 2002 and 2006 and to the Swedish Hybrid Vehicle Centre, SHC, from year 2007.

I would like to express my gratitude to all people involved, especially my academic supervisor Professor Annika Stensson Trigell at KTH and my industrial supervisor Dr. Anders Bodin at Hägglunds for their support and incessant encouragement during the entire project. I also want to thank Johan Wedlin at Volvo Cars (now at AB Volvo), Lars Carlhammar at Volvo Technology, Rajiv Gupta at General Motors, Gunnar Olsson at Saab Automobile, Mats Jonasson at Volvo Cars and Leo Laine at Volvo 3P for valuable comments and feed-back during the steering committee meetings. Göran Johansson and Sture Eriksson also deserve credit for keeping up good spirits within the FCHEV framework.

Olof Noréus
Örnsköldsvik, October 2010

Appended papers

Paper A

Six-wheeled vehicle steering.
O. Noréus
Presented at the 15th International Conference of the ISTVS, Hayama, Japan September 25–29, 2005.
Published in Proceedings of the 15th International Conference of the ISTVS.

Paper B

Simulation of electric transmission for off-road vehicle.
O. Noréus
Presented at the 15th International Conference of the ISTVS, Hayama, Japan September 25–29, 2005.
Published in Proceedings of the 15th International Conference of the ISTVS.

Paper C

Tire/terrain models for simulating six-wheeled vehicle on soft ground.
O. Noréus
Presented at the 10th European Conference of the ISTVS, Budapest, Hungary October 3–6, 2006.
Published in Proceedings of the 10th European Conference of the ISTVS.

Paper D

Measurement of terrain values and drawbar pull for six wheeled vehicle on sand.
O. Noréus and A. Stensson Trigell
Presented at the 16th International Conference of the ISTVS, Turin November 25–28, 2008
Published in Proceedings of the 16th International Conference of the ISTVS.

Contribution of authors: *Noréus planned and supervised the experiments, did the analysis and the presentation at the conference. Noréus and Stensson Trigell wrote the paper.*

Paper E

Comparison of measured and simulated drawbar pull for six wheeled vehicle with radial pneumatic tyres on sand.
O. Noréus and A. Stensson Trigell
Submitted for publication in Journal of Terramechanics.

Contribution of authors: *Noréus suggested and developed the tyre model, performed the simulations and did the analysis. Noréus and Stensson Trigell wrote the paper.*

Paper F

Control of at-the-limit handling behaviour of a six-wheeler: strategies based on individual steer and individual torque control.
O. Noréus and A. Stensson Trigell
Submitted for publication in Vehicle System Dynamics.

Contribution of authors: *Noréus designed the driving scenarios, suggested and developed the control strategies, performed the simulations and did the analysis. Noréus and Stensson Trigell wrote the paper.*

Contents

Chapter 1

Background

1.1 Improving performance for six-wheeled vehicles

There are many aspects of improving the performance for six-wheeled vehicles. One important property is the ability to steer. Since there are six wheels, it is possible to apply steering angles in different ways to achieve good steering performance [1, 2, 3]. A different approach is to use individual wheel torque control to improve steering [4].

Another aspect is improving performance in terrain, for example by designing the suspension [5] and evaluate mobility in soft terrain [6].

1.2 Objectives

Development of hybrid electric vehicles is very complex and methods for speeding up the development process are therefore needed. To be able to predict and understand effects of different design solutions on vehicle performance, dynamic models of the vehicle and the environment need to be developed. The dynamic vehicle model is important for simulation of handling characteristics in different situations, and it is also crucial for the development of control laws for vehicle subsystems. The dynamic vehicle model will also be invaluable as a test bed for a variety of vehicle operating strategies. The importance of simulation is increasing with the frequent appearing non-linear properties of vehicle components.

There are more possibilities to control the propulsion in a vehicle with an electric transmission compared to a vehicle with conventional internal combustion engine and mechanical transmission. With independent wheel stations with in-hub electric motors it is possible to control propulsion, steering and suspension individually for each wheel, which makes it possible to improve mobility, performance and driving safety. This work focuses on modelling of driving dynamics aspects of a six wheeled electric transmission vehicle, and the long term goal is to develop a method that can evaluate the mobility in terrain. This is made by combining modelling of vehicle, transmission and terrain behaviour.

1.3 Research problem

The overall research question is the following:

- Which modelling environment is needed to enable analysis of the driving dynamic performance of six-wheeled hybrid electric vehicles both on- and off-road?

1.4 Outline of thesis

In addition to the appended papers, this thesis has a main body to give the reader an introduction to the subject, and more thoroughly present the findings. The main body is divided into 9 chapters, where the present chapter describes the thesis background. Chapter 2 gives an introduction on terrain vehicles. The work on vehicle modelling and tyre/terrain models is presented in Chapter 3. Performed measurements, both to provide model input and to be able to compare simulation results to real data, are described in Chapter 4. Simulation results are presented in Chapter 5 and appended papers are discussed in Chapter 6. The main scientific contribution of the work is explained in Chapter 7 and Chapter 8 contains conclusions of this work. Finally, recommendations to future work are presented in Chapter 9.

Chapter 2

Terrain vehicles

2.1 Tracked vehicles

In order to be able to drive a vehicle off-road, the vehicles need higher ground clearance and lower ground pressure than ordinary road vehicles. The higher ground clearance is needed when climbing over obstacles and when running in deep snow to get the wheels down to firm ground to get grip. When driving on soft ground the lower ground pressure is needed to avoid sinking down and getting stuck. Tracked vehicles provide low ground pressure and have great mobility on soft terrain. They may be able to travel both over snow and marshland. Tracked vehicles with two tracks are skid-steered, i.e. in order to turn, the outer track is driven faster than the inner track. There are also two-car articulated vehicles with four tracks. When driving on roads, tracked vehicles will have larger rolling resistance and the terrain tracks will cause more noise and vibrations than wheeled road vehicles.

2.2 Wheeled vehicles

When driving on soft terrain it is important to keep the ground pressure down in order not to get stuck. On firm ground, the ground pressure usually is not that important, but most tyres have an upper limit on the load they can carry. Therefore it might be necessary to increase the number of wheels on heavy vehicles as for example on some heavy buses and trucks. While the increased numbers of wheels are reducing both the vertical load of the tyres and the ground pressure, they also contribute to the total weight of the vehicle. In particular that

is true for terrain vehicles where it is desired to be able to drive on all wheels and more gear boxes and drive shafts or electric motors are needed. In order to get better obstacle climbing performance, wheeled terrain vehicles usually have large and soft tyres with terrain treads. Heavy off-road wheeled vehicles often have six or eight wheels in order to distribute the load in order to avoid exceeding the maximum tyre load and get larger ground contact area. Wheeled terrain vehicles can usually run in snow with depth up to the wheel radius and on sand and soil as long as it is not too soft and climb over obstacles, but they do not provide as good terrain mobility as tracked vehicles, e.g. they cannot run over snow and on marshland. On the other hand, wheeled terrain vehicles instead have much better performance on road, with lower rolling resistance, less noise and vibration as well as better high-speed manoeuvrability. In order to get reasonable good performance both on- and off-road, a six-wheeled vehicle is chosen for this application.

Chapter 3

Modelling of six wheeled vehicles and tyre/terrain interaction

The purpose of a vehicle is to move the vehicle body according to the driver's commands. In Figure 3.1 a schematic figure of ingredients in the proposed model of a wheeled vehicle on both on- and off-road is illustrated. It is shown that the driver's controls are the accelerator pedal and the steering wheel, affecting the powertrain and the steering system, respectively. Usually a brake pedal is also an important control, but it is not included in this model, since no braking manoeuvres have been evaluated here. However, both positive and negative torque can be applied on the drive motors, and in Chapter 5.5 it is described how braking torques are applied on some of the wheels.

When driving on-road with wheeled vehicles, torque feedback from the steering system, indicated by grey arrows in Figure 3.1, provides valuable information to the driver. In [7], driving simulator experiments show that no drivers participating in the experiment were able to drive properly without steering wheel torque feedback. For off-road driving on the other hand, torque feedback to the steering wheel is usually a drawback, since it increases the driver effort to keep the desired steering angles, and the driver might even get hurt if the steering wheel starts spinning when running over obstacles. Since the focus here is vehicle behaviour rather than driver behaviour, torque feedback in the steering system is not included in the model.

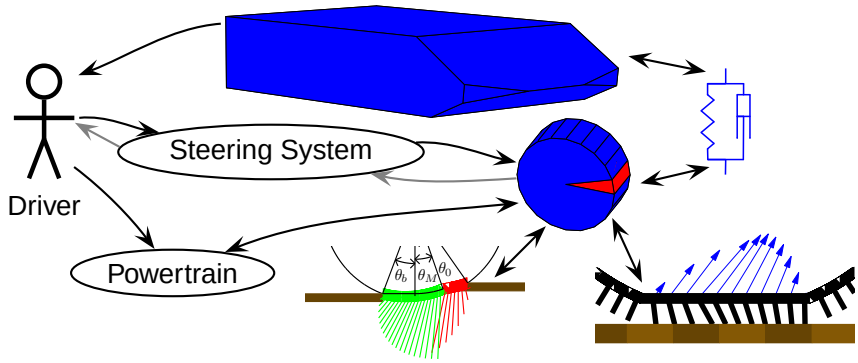

Figure 3.1: Schematic figure of the complete model. Depending on the vehicle, some of the subsystems should be multiplied. The vehicle considered in this work contains six wheels with drive motors and two diesel engines with generators.

To perform the manoeuvres in the evaluations, a rather simple driver is applied that model uses the vehicle body velocity and heading to control the accelerator pedal and the front axle steering angle. The driver model is not intended to behave like a human driver, but rather to perform manoeuvres that makes it easy to evaluate different vehicle control strategies.

The powertrain is assumed to be an electric transmission, where the power source is a diesel engine, providing mechanic energy to the generator. In the generator, the mechanic energy is converted to electric energy. The alternating current from the generator is rectified and then a power inverter is used to feed the drive motor, which converts the electric energy to mechanic energy by providing the wheel with a torque. The amount of torque is determined by a control system, which uses the accelerator pedal as input.

Both the steering system and the powertrain interacts with the wheels, which in turn interact with the ground. Two different kinds of models are developed for the ground interaction, depending on if the ground is soft or rigid.

To close the loop, the wheel interacts with the vehicle body via the suspension. As the vehicle body moves, it provides feedback to the driver model.

3.1 Vehicle model

The vehicle body is modelled as a rigid body with a coordinate system according to Figure 3.2. As can be seen in the figure, x corresponds to longitudinal

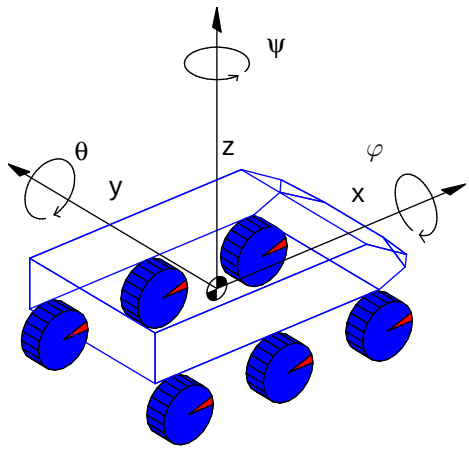

Figure 3.2: Coordinate system.

position, y is lateral position, while z is vertical position. Yaw, pitch and roll angles are represented by ψ, θ and φ respectively.

The complete vehicle model is shown in Figure 3.3. Each wheel has a mass and inertia and is connected to the vehicle body by a spring and damper. Furthermore, they can rotate along their y-axis and are steerable along their z-axis. This means that each wheel has three degrees of freedom. Since the vehicle body has six degrees of freedom and there are six wheels, the complete model has 24 degrees of freedom. The interaction between the tyres and the ground are illustrated by springs and dampers that are only active as the tyre is sufficiently close to the ground, i.e. they can only produce reaction forces in the positive z-direction of the wheels as they are in contact with the ground.

The geometry of the vehicle model used in the simulations and the definition of β is shown in Figure 3.4

In *Paper A*, where steering characteristics are in focus, the suspension is assumed to be rigid and each pair of wheels are mechanically connected such that there are only three parameters for determining the steering angles for all wheels. Thus, the model has 15 degrees of freedom in this case. The ground is assumed to be rigid and in order to be able to simulate the load distribution between different wheels the tyres are assumed to be elastic, which is simulated by dampers and springs that can only generate forces to lift the tyres from the ground, not pulling them down. In addition to that simplified vehicle model also a detailed model with the complete suspension geometry is used for validation.

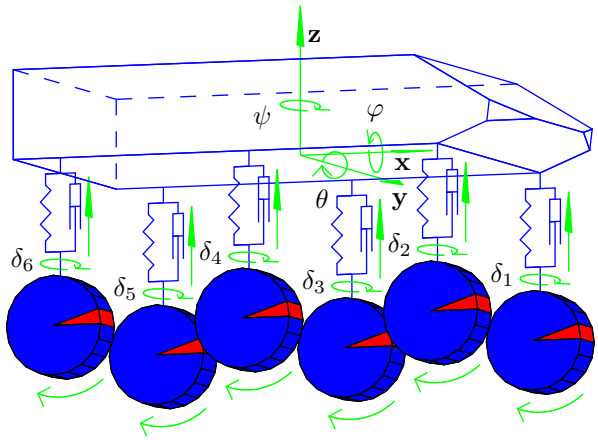

Figure 3.3: Complete vehicle model with springs and dampers. The vehicle model has 24 DOF, excluding the tyre model.

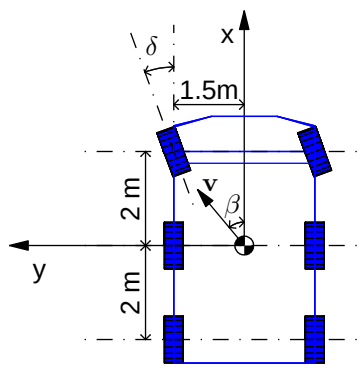

Figure 3.4: Vehicle geometry and definition of β.

Since the focus in *Paper B* is to simulate the electric transmission and no steering manoeuvres are considered, a simple one dimensional vehicle model is used, where only Newton's second law, rolling resistance and air resistance are included. Thereby, the simplified vehicle model in this case only has one degree of freedom.

In *Paper C*, which focus on tyre/terrain modelling, the wheels are rigid in the model for terrain simulations, which is a good approximation as long as the ground pressure is low compared pressure from the air in the tyres and the tyre carcass, resulting in low tyre deformation. Since the terrain is elastic and the terrain models simulate forces in all three dimensions, there is no need to have elasticity in the tyres for simulation reasons as in *Paper A* either. There is a spring and damper characterising each wheel as in Figure 3.3. The front and rear pair of wheels are steered and each pair of wheels are connected such that there is one steering angle parameter for the front wheels and one steering angle parameter for the rear wheels. Thus, the model has 20 degrees of freedom.

The tyre/terrain model is further developed in *Paper E*, in order to simulate pneumatic tyres on soft ground. Drawbar pull measurements are performed in *Paper D*. Since no lateral forces are needed to do comparisons between measurements and simulations, no steering angles are applied and the model is therefore reduced to 18 degrees of freedom.

To evaluate at-the-limit handling in *Paper F*, different manoeuvres are simulated on rigid, low friction ground. To get physically reasonable tyre forces during large combined slips, a brush tyre model is implemented. Steering is performed on the front axle, and optionally also on either the middle or rear axle. Hence, the vehicle model does not exceed 20 degrees of freedom.

3.2 Steering model

Steering is here considered to be performed by applying a steering angle δ to the wheels. However, on a six-wheeled vehicle steering can be done on different pair of wheels and combinations of several pair of wheels and it is not clear which solution is optimal.

The different approaches to achieve steering include:

- Skid steering
- Steering on front wheels

- Steering on front and intermediate wheels
- Steering on front and rear wheels
- Steering on all wheels.

The considered steering methods in *Paper A* are steering on front wheels, steering on front and intermediate wheels and steering on front and rear wheels. Skid steering, i.e. steering by applying different torques to the wheels, is not considered since it is assumed that a conventional steering system is needed in order to get a vehicle that behaves and feels like conventional wheeled vehicles and also for safety reasons since it is possible to use muscle power to operate a conventional steering system if the power is lost. Steering on all wheels is avoided since more actuators and large wheel housings would be needed for all wheels. For more details on the modelling, see *Paper A*.

3.3 Model of electric transmission

For six-wheeled vehicles an electric transmission with in-hub motors is an interesting alternative to conventional mechanical transmissions. Since a lot of gearboxes and drive shafts are needed with a mechanical transmission in order to get all wheel drive, the electric transmission is weight competitive and it also makes it possible to get redundancy by using two diesel engines as power sources in an uncomplicated manner. In the mobility perspective the electric transmission is interesting since the torque can be controlled individually for each wheel. No extra actuators or sensors are needed for the torque control since this is an inherent quality of the electric transmission.

The electric transmission makes it possible to add energy storage, e.g. batteries or ultra capacitors, to get a hybrid electric vehicle and that enables silent drive with the diesel engines shut off and to use regenerative braking in order not to waste the brake energy.

In Figure 3.5 the complete model, presented in *Paper B*, including one diesel motor, a generator, DC-bus, traction motor and the vehicle represented by an inertia, a rolling resistance and air resistance is shown. The control system consists of a speed controller for the diesel engine, a generator controller, traction motor controller and one main controller for the powertrain. There is no energy storage except for the DC bus capacitance in this model, which means that it is not possible to use more power than the diesel engine can produce.

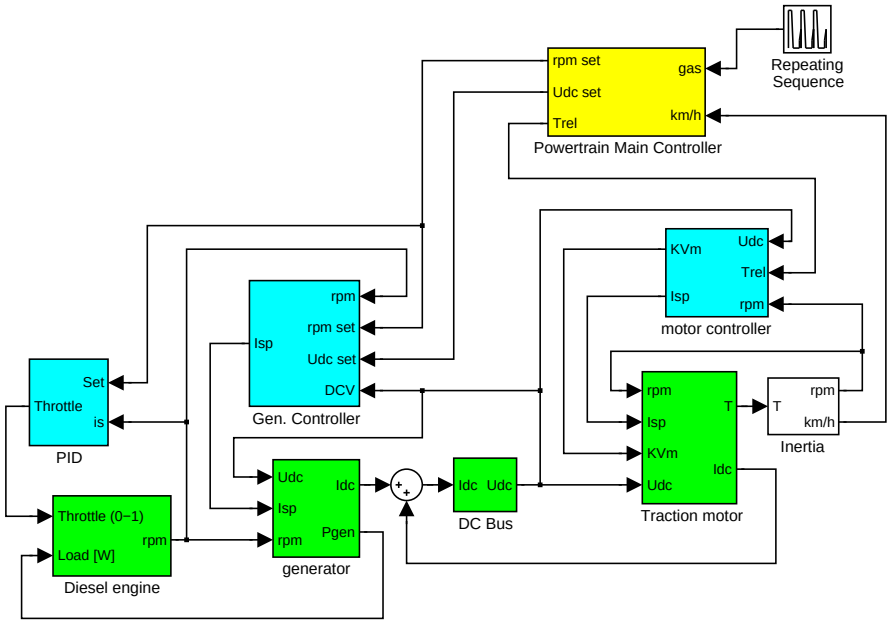

Figure 3.5: Model for the complete electric transmission system.

The models derived in *Paper B* are not very detailed, since the purpose is to use them in vehicle dynamics simulations to get realistic boundaries for what the drive motors can produce and to make it possible to simulate the control architecture.

The considered diesel-electric transmission consists of a diesel engine, generator, rectifier, a DC link, converter and drive motor. The vehicles considered in this work have two diesel engines with one generator each and there are six drive motors on wheeled vehicles and at least two motors for tracked vehicles. For simplicity only one diesel engine and one drive motor have been simulated. A controlled rectifier is considered and both the generator and drive motor are supposed to be permanent magnet machines. For more details on the modelling, see *Paper B*.

There are parallel hybrid electric vehicles with a mechanical drive shaft from the engine to the wheels described in [8], but since there is no mechanical drive shaft between the diesel engine and the drive motor in the vehicle considered here, it is close to a series hybrid vehicle described by [9] and [10], but it has no energy storage.

3.4 Tyre and terrain models

3.4.1 Rigid ground

Tyre models for tyres running on road assume that the ground is rigid and that all deformation will take place in the tyre structure. One example is the Dugoff tyre model used for example in [1] and *Paper A*. Most models are intended for cars which have low deflections in the tyres. A model that can handle large deflections in off-road tyres is developed by [11].

3.4.2 Brush model for tyre on rigid ground

When evaluating at-the-limit handling, the vehicle is assumed to be running on a low friction, flat and rigid surface. All deformation is therefore taking place in the tyres. As the tyres will be running in high combined slip conditions, it is important that the tyre model predictions are physically reasonable during those conditions. Since the vehicle is a terrain vehicle, tyre parameters for conventional tyre models like Pacejka's magic formula [12] are hard to get. Therefore, the brush tyre model is chosen in this case, since it is a relatively simple physical model. The model is described in detail in [12, 13] and only a short overview is given here.

In the brush tyre model, the tyre tread that is in contact with the ground is modelled as bristles. In Figure 3.6, the tyre rolling direction is to the right and the tyre is driving, i.e. the tyre slip, s, is positive. In the contact area the tyre is deformed to a flat area and the pressure distribution is assumed to be parabolic,

$$q_z = \frac{3F_z}{4a}\left(1 - \left(\frac{x}{a}\right)^2\right), \tag{3.1}$$

where F_z is the vertical force between the tyre and the ground, a is half the length of the contact region and x is a longitudinal position in the contact region. Equation 3.1 is a common assumption, e.g. proposed in [12].

Due to the pressure q_z, there will be a normal force, perpendicular to the ground, acting on each bristle. Since the wheel is driven to the right in Figure 3.6, the tyre carcass will move to the left with respect to the ground, and due to the bristle stiffness, there will be a shear stress, τ_x acting on each bristle. At low tyre slip, there will be an adhesive region, where $\tau_x \leq q_z\mu_s$, and for $s \neq 0$ there is a sliding region where $\tau_x = q_z\mu_k$, where μ_s and μ_k are, respectively, the static and kinetic coefficients of friction.

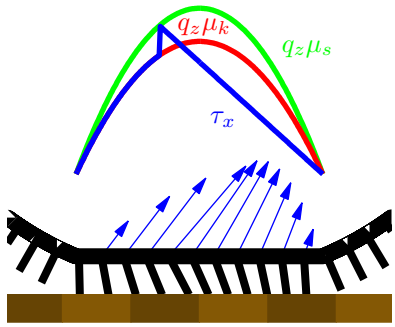

Figure 3.6: Shear stress and normal load distribution in the brush tyre model for pure longitudinal slip.

The tyre slip is pure longitudinal, positive and small enough to keep an adhesive region in the contact patch in Figure 3.6, and it can be seen in the figure that the deformation of the bristles is increased in the adhesive region until $\tau_x = q_z\mu_s$ and the bristles start sliding.

For simplicity, isotropic sliding friction is assumed when calculating tyre forces for combined slips. Different methods to calculate tyre forces for different friction behaviour assumptions are described in [13].

3.4.3 Rigid wheel on soft ground

As long as the terrain is soft compared to the pressure in the tyre, it is possible to assume that the tyre is rigid. This is true when the pressure from the tyre due to the inflation pressure and the carcass pressure is higher than the ground pressure, which is further discussed in [14] and [15]. However, a tyre does not necessarily behave like a rigid wheel just because the inflation pressure is higher than the ground pressure, which is shown in Chapter 3.4.4.

The ground pressure, σ, beneath the tyre in the contact area can be derived from relationships between sinkage and pressure, such as the relationship proposed by Bekker,

$$\sigma = \left(\frac{k_c}{b} + k_\phi\right) z^n, \tag{3.2}$$

where z is the sinkage, b is the dimension of the loading area, e.g. the width of a rectangular plate or the radius of a circular plate, and k_c and k_ϕ are terrain values with units depending on the terrain value n. This approach is described in [15]. The terrain values can be determined with the Bevameter technique.

With a Bevameter two types of tests are performed, a normal pressure-sinkage test and a shear test. In the normal pressure-sinkage test a plate is pressed down and the pressure is measured as a function of the sinkage of the plate. The shear test is performed with shear rings. Internal shearing is measured by using grousers and external shearing by using a rubber coated shear ring. The Bevameter technique is further described in [16].

Reece proposed an alternative to Equation 3.2 for the relationship between sinkage and pressure,

$$\sigma = \left(ck'_c + \gamma b k'_\phi\right)\left(\frac{z}{b}\right)^n \tag{3.3}$$

A benefit with this relationship is that the units of the constants k'_c and k'_ϕ are independent of the value of n. The models developed in this work are derived from this relationship.

The pressure under a rigid tyre on soft ground can be described in a similar way, but when the wheel is driven the highest pressure will not be where the highest sinkage is. There will be two flow zones around the tyre since the soil in front of the wheel will flow forwards and the soil under the wheel will flow backwards. The highest soil pressure will occur between these two flow zones. Exactly where the maximum pressure will be located, θ_m, is depending on both the type of soil and the slip. For sand, [17] give the expression

$$\theta_m = \theta_0 \left(c_1 + c_2 s\right), \tag{3.4}$$

where c_1 and c_2 are empirical constants depending on the type of terrain and the slip is defined as

$$s = 1 - \frac{v}{r\omega}, \tag{3.5}$$

where v is the velocity, r is the radius and ω is the angular speed of the tyre.

A tyre on soft ground is shown in Figure 3.7. The soil is deformed plastically such that the level is lower after the wheel has passed. As the soil is compressed a pressure is built up. In the front part of the ground contact area of the tyre, the pressure will rise from zero at θ_0 and increase to the maximum point θ_m. It is assumed that the pressure is symmetric in the two parts of the contact area with respect to the relative position in the areas. Therefore, the pressure is expressed as

$$\sigma = \begin{cases} \sigma_1, & \theta \geq \theta_m \\ \sigma_2, & \theta < \theta_m \end{cases}, \tag{3.6}$$

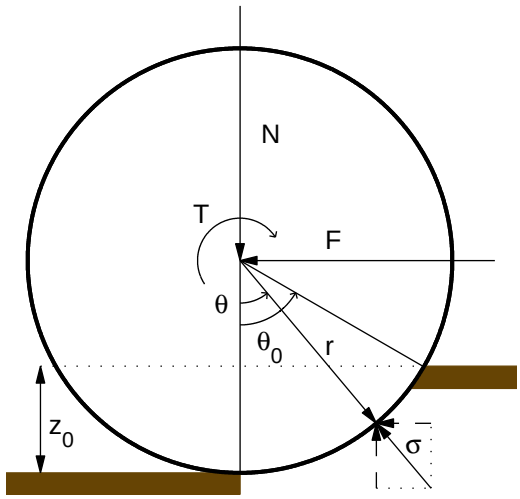

Figure 3.7: Model for driven wheel on soft ground.

where

$$\sigma_1 = \left(k_c' + k_\phi' b\right)\left(\frac{r}{b}\right)^n (\cos\theta - \cos\theta_0)^n \tag{3.7}$$

$$\sigma_2 = \left(k_c' + k_\phi' b\right)\left(\frac{r}{b}\right)^n \left(\cos\left(\theta_0 - \frac{\theta}{\theta_m}(\theta_0 - \theta_m)\right) - \cos\theta_0\right)^n \tag{3.8}$$

according to [17].

Since σ_1 is independent of s, the pressure distribution in the front of the maximum pressure position, i.e. the part of the tyre where $\theta \geq \theta_m$, is also independent of s. However, θ_m and the pressure distribution in the rear part of the tyre will vary with the slip, which is shown in Figure 3.8.

According to [17] and [15] and originally proposed by [18], the shear stress around the rim can be expressed as

$$\tau(\theta) = (c + \sigma(\theta)\tan\phi)\left(1 - \mathrm{e}^{-j/K}\right). \tag{3.9}$$

In order to handle lateral forces, the shear deformation along the soil-wheel interface has to be handled both in the longitudinal and lateral direction of the tyre, i.e.

$$j = \sqrt{j_s^2 + j_y^2}, \tag{3.10}$$

where

$$j_s = r\left((\theta_0 - \theta) - (1 - s)(\sin\theta_0 - \sin\theta)\right), \tag{3.11}$$

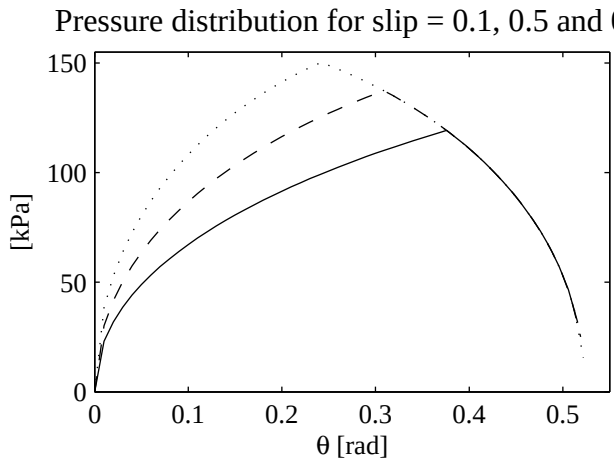

Figure 3.8: The pressure distribution beneath the tyre contact area for slip 0.1 (dotted line), 0.5 (dashed line) and 0.9 (solid line). In this case θ_0 is set to be the same independently of the slip and the vertical force due to the ground pressure will thereby be reduced as the slip is increased.

according to [17] and

$$j_y = v_y \frac{\theta_0 - \theta}{\omega}. \tag{3.12}$$

The radial ground pressure and the shear stress give rise to both vertical and horizontal forces

$$N = rb \int_0^{\theta_0} \sigma(\theta) \cos\theta + \tau_s(\theta) \sin\theta \, \mathrm{d}\theta \tag{3.13}$$

$$F_x = rb \int_0^{\theta_0} \tau_s(\theta) \cos\theta - \sigma(\theta) \sin\theta \, \mathrm{d}\theta, \tag{3.14}$$

according to [17], while, due to the lateral shear stress, there is a lateral force

$$F_y = rb \int_0^{\theta_0} \tau_y(\theta) \, \mathrm{d}\theta. \tag{3.15}$$

In Figure 3.9 the shear stresses in the soil-wheel interface are shown.

The edge effect on the deformation when soil is entering and leaving the soil/wheel interface on the side of the tyre is disregarded. The lateral force due to "bulldozing" as the tyre moves in the lateral direction described in [19] is also ignored.

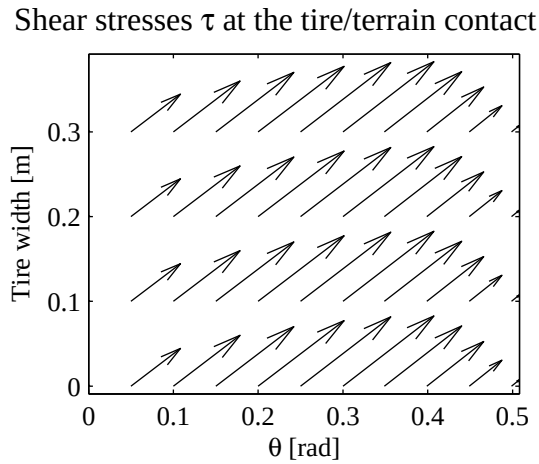

Figure 3.9: Shear stresses beneath the tyre contact area for $s = 0.5$, $\alpha = 0.2$ rad. The y-axis represents the width of the tyre and the x-axis represents the longitudinal direction of the contact area. Zero corresponds to the point below the wheel centre and in this case $\theta_0 = 0.5$ rad.

Due to the longitudinal shear force, there also will be a torque on the wheel,

$$T = r^2 b \int_0^{\theta_0} \tau_s(\theta)\, \mathrm{d}\theta. \tag{3.16}$$

In the simulations, the torque in Equation 3.16 and the torques from the drive motors are used in order to simulate the angular accelerations of the wheels.

Damping characteristics of the terrain is not included, which means that the models are not suitable for transient simulations, or at least the results might not be valid during transients.

By varying the slip it is possible to plot friction ellipses for different steering angles. In Figure 3.10 parts of the friction ellipses are plotted for positive slips and steering angles. Since the horizontal part of the ground pressure give rise to a force in opposite direction of the tyre movement, the rolling resistance is inherent in the tyre model and it is therefore included in the tyre forces. That is why there are negative longitudinal forces although the slip is never negative in the figures. The slip is zero at the left parts of the lines and is increased to one in the lower right end of the lines, where the lateral force is zero. When the slip is low, the longitudinal force is negative, which means that the rolling resistance is higher than the tractive force generated by the tyre. The lateral force is depending both on the slip angle, α, and the slip. A larger slip angle

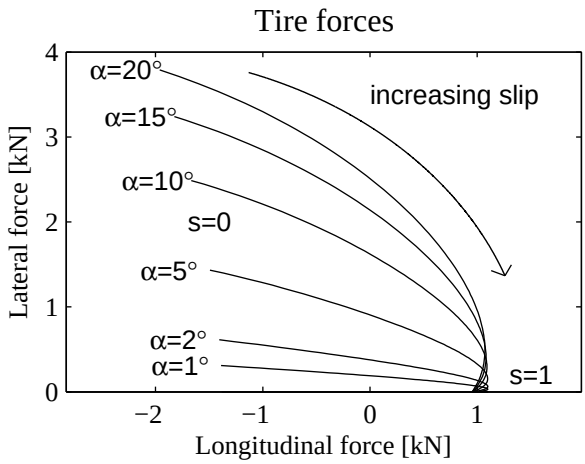

Figure 3.10: Longitudinal and lateral forces when the slip is varied from 0 at the left part of the lines to 1 at the lower right end of the lines at different steering angles.

generates a higher lateral force, but as the slip is increased to 1, the lateral force always approaches 0.

3.4.4 Pneumatic tyre on soft ground

When using pneumatic tyres on soft ground, both the tyres and ground have the ability to be deformed. The tyre shape in the contact area depends on the stiffness of both the soil and the tyre. The deformation of the tyres improves the mobility since the contact area with the ground is increased, while the maximum ground pressure is decreased.

A common assumption, used for example by Qiao [20], is that the tyre surface pressure never exceeds the combination of the carcass stiffness and internal tyre pressure. In [21], the tread belt is analysed in the circumferential direction to define a limit pressure, at which the tyre starts deforming. As the limit pressure is exceeded, a straight line is inserted, saturating the radial stresses to the limit pressure.

Fujimoto [22] describes several different assumptions for flexible tyre shapes. The extremes are easily understandable; a soft tyre on rigid ground will form a horizontal surface, while the soil will adapt to the shape of the wheel when a rigid wheel is running in soft terrain. Among the more interesting suggestions for shapes in-between the extremes are an assumption to let the tyre have a horizontal flat surface, as if the tyre was running on rigid ground, at the depth of the

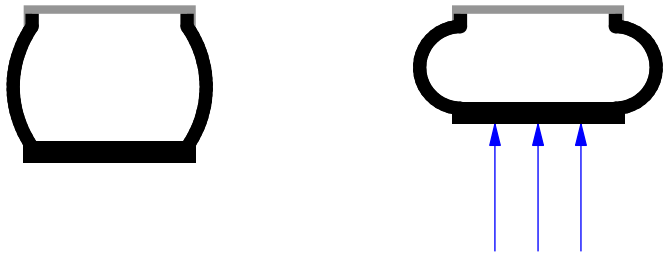

Figure 3.11: Tyre cross section with flexible sidewalls and rigid tread. Equilibrium without ground pressure to the left, deformation as ground pressure is applied to the right.

tyre rut, which makes it easy to predict the tyre performance. Another assumption is to let the tyre mimic a rigid wheel with larger radius at the tyre/terrain contact area making it easy to use the theory for rigid wheels.

However, since the vehicle used for the experiments in this paper is equipped with radial tyres, a different method for deriving the tyre deformation and surface pressure is proposed here. A tyre cross section is analysed and it is assumed that the tension in the tyre sidewall, rather than the circumferential tension in the tread belt, is determining the deformation of the tyre. Moreover, since the relation between the tyre deformation and the surface pressure of the tyre is determined, the shape of the tyre and terrain interface is identified by finding the equilibrium between the tyre surface pressure and the normal stresses in the ground.

To find the tyre stiffness, the tyre cross section shown in Figure 3.11 is used to make a simplified model, similar to the load carrying description in [23]. The bending stiffness of the tread part is assumed to be rigid in the lateral direction, but flexible in the circumferential direction of the tyre. The sidewalls are assumed to be of constant length, i.e. they are inextensible and won't stretch. However, they are assumed to be flexible and easily bend and adopt to a circular arc shape due to the tyre pressure.

Considering the forces acting on the tread part in Figure 3.12 and the sidewall part in Figure 3.13, we get the system of equations defined by

$$\uparrow: \quad f_s \cos\frac{\theta_s}{2} = \frac{b}{2}(P_t - \sigma) \tag{3.17}$$

$$\leftarrow: \quad f_s \sin\frac{\theta_s}{2} = P_t \frac{h_s}{2}. \tag{3.18}$$

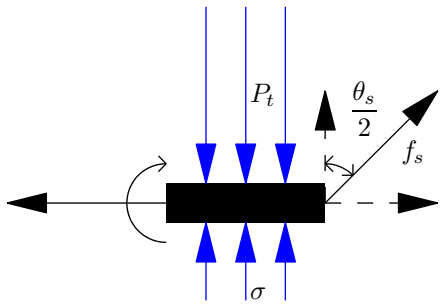

Figure 3.12: Free body diagram for the rightmost half part of the tread of a tyre.

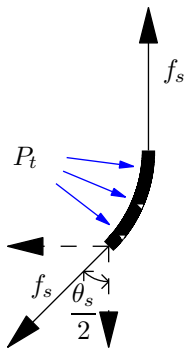

Figure 3.13: Free body diagram for the lower part of the tyre sidewall.

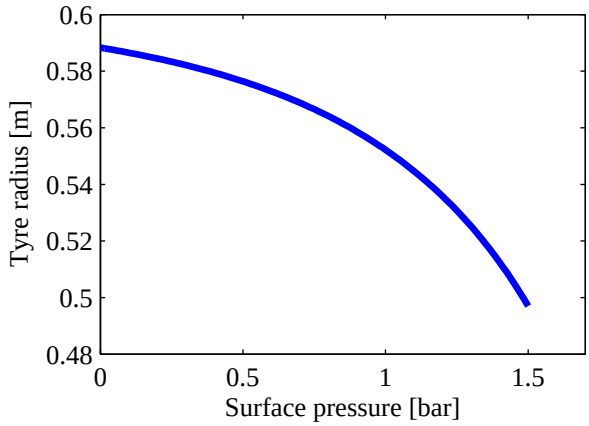

Figure 3.14: Tyre radius versus surface pressure for tyre pressure of 1.5 bar. Although the surface pressure on the tyre does not exceed the tyre pressure, there is a significant deformation of the tyre.

Dividing Equation 3.18 by Equation 3.17 yields

$$\theta_s = 2 \arctan \frac{P_t h_s}{b\,(P_t - \sigma)}, \tag{3.19}$$

i.e.

$$\sigma = P_t - \frac{P_t h_s}{b \tan \frac{\theta_s}{2}}. \tag{3.20}$$

Since

$$h_s = 2 \frac{l_s}{\theta_s} \sin \frac{\theta_s}{2}, \tag{3.21}$$

we get

$$l_s = \frac{\theta_s h_s}{2 \sin \frac{\theta_s}{2}}. \tag{3.22}$$

For an unloaded tyre, i.e. $\sigma = 0$, it is now possible to insert b and h_s into Equation 3.19 and then into Equation 3.22 to calculate the constant l_s. Now, since l_s is known, h_s can be calculated for every possible θ_s using Equation 3.21. Then it can be inserted into Equation 3.20 to get the corresponding external surface pressure on the tyre, σ. The calculations are performed for a 405/70 R24 tyre, and the result is shown in Figure 3.14.

To find the shape of the tyre/terrain interface, the appropriate ground sinkage is found in order to get the tyre surface pressure in Figure 3.14 to match the ground pressure. As for the rigid wheels in Chapter 3.4.3, the ground pressure

is assumed to be depending on the sinkage, but since the tyre radius is varying for a flexible tyre, Equations 3.7 and 3.8 are modified to

$$\sigma_1 = \left(k'_c + k'_\phi b\right)\left(\frac{z(\theta)}{b}\right)^n \tag{3.23}$$

$$\sigma_2 = \left(k'_c + k'_\phi b\right)\left(\frac{z\left(\frac{(\theta_m-\theta)(\theta_0-\theta_m)}{\theta_m+\theta_b} + \theta_m\right)}{b}\right)^n, \tag{3.24}$$

where $z(\theta)$ is found by assuming the tyre surface pressure to be in equilibrium with the ground pressure. The position of the maximum pressure, θ_m, is determined by an approach similar to the method for the rigid wheels in Chapter 3.4.3. However, due to the deflection of the tyre, the angle between the tyre surface and the undisturbed soil surface is lower in the front area, i.e. the normal stresses have a lower horizontal component, while the shear stresses have a larger horizontal component. On the rear contact area on the other hand, the angle is increased as the tyre is expanding due to the decreasing ground pressure.

The increased angle of the rear zone will prevent the soil from flowing backwards, and the position of the maximum pressure, θ_m, is therefore assumed to be where the principal stress is vertical in the rear zone, which is shown in Figure 3.15. A similar tyre shape is shown in [24], where the pneumatic tyre shape is measured when moving in dry sand.

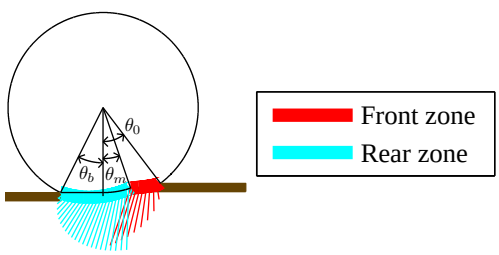

Figure 3.15: Side profile of flexible tyre on soft ground. The lines beneath the wheel show the resultant of the ground pressure and shear stresses in the rear and front zone.

The radial ground pressure and the shear stress give rise to both vertical and horizontal forces. Since the tyre is not circular in this case, the ground pressure is assumed to be perpendicular to the tyre surface. Thus, θ_i is used to denote

the angle between the tyre surface and the undisturbed soil surface to get

$$N = b \int_{-\theta_b}^{\theta_0} \frac{r}{\cos(\theta - \theta_i)} (\sigma \cos\theta_i + \tau_s \sin\theta_i) \, \mathrm{d}\theta \tag{3.25}$$

$$F_x = b \int_{-\theta_b}^{\theta_0} \frac{r}{\cos(\theta - \theta_i)} (\tau_s \cos\theta_i - \sigma \sin\theta_i) \, \mathrm{d}\theta. \tag{3.26}$$

The wheel torque is calculated similarly as for the rigid wheel in Equation 3.27, but adjusting the lower integration limit to include the extended contact area rear of the wheel centre for the flexible tyre, to get

$$T = r_w^2 b \int_{-\theta_b}^{\theta_0} \tau_s(\theta) \, \mathrm{d}\theta. \tag{3.27}$$

The tyre circumference is assumed to be a constant independent of the tyre inflation pressure, i.e. the tyre rolling radius is independent of the inflation pressure, which is also confirmed by the measurements. Since the tyre circumference is assumed to be constant, the tyre tread is running at the same velocity, only depending on the angular speed of the wheel, independent from the tyre inflation pressure. Considering the law of energy conservation and neglecting the tyre losses, the force at the tyre tread has to be related to the wheel torque by the same constant, i.e. the tyre rolling radius, r_w, independently of the inflation pressure. Hence, the tyre rolling radius is used when determining the torque in Equation 3.27.

Chapter 4

Measurement methods

4.1 Measurement of tyre deformation on flat, rigid ground

When driving on soft terrain, it is beneficial to lower the tyre pressure to get a larger tyre/terrain contact area and thereby a lower ground pressure, which improves the drawbar pull. However, the pressure must not be too low, since the mobility is affected negatively if the rim, run flat or mine protection inserts interferes with the ground. The risk of damaging the tyre or rim also increases if that happens. Therefore, it is useful to know how much the tyre is deformed at different tyre pressures. In this thesis, the measurement is of particular interest since it enables the possibility to compare the pneumatic tyre model described in Section 3.4.4 to real data.

To measure the tyre pressure influence on tyre deformation, the shortest distance from the rim to the ground is measured for an unloaded tyre and a loaded tyre. The difference is calculated to get the tyre deformation,

$$\Delta h_s = h_s^0(P_t) - h_s(P_t), \tag{4.1}$$

where Δh_s is the tyre deformation, h_s^0 is the distance from the rim to the ground for the unloaded tyre, h_s is the corresponding distance for the loaded tyre and P_t is the tyre pressure.

4.2 Pivot turning performance

Pivot turning is a method to simplify turning in narrow areas. Since the pivot turning speed affects the time it takes to perform manoeuvres in narrow areas, it is an important part in the specification of the performance of a vehicle. Here, the measurement is mainly interesting since it makes it possible to do simulations with the tyre model described in Section 3.4.2 and compare to real data measured during large combined slips conditions.

The pivot turning performance is characterised by the time necessary to perform the pivot turn. Normally, except for demonstration purposes, it is not useful to turn more than 180°, since the pivot turn involves excessive tyre wear and is supposed to be used to quickly change the direction of travel in narrow areas. However, as a compromise between tyre wear and to get a reasonable accuracy in the measurements, the time is measured during a steady state 360°. In that way, also influence from rise times in the powertrain are avoided.

Ideally, measurement rims should be used in order to measure wheel torques during the pivot turn, to be able to simulate the pivot turn during reasonable similar conditions. More indirect methods include measuring the hub motor power consumption or to determine the combustion engine power from the engine speed, power command and engine map. Due to the losses in the transmission, the mechanical power on the wheels will be lower than the measured power. Here, either the power consumption of the hub motor inverters or the estimated diesel engine power have been able to use, depending on what measurements are possible to perform at the time. The estimated power losses to the wheels are then subtracted.

4.3 Measurement of terrain values and drawbar pull

In order to be able to validate the proposed soft ground tyre/terrain interaction models, experiments are performed to measure vehicle performance on a terrain with known characteristics. One challenge when performing terrain measurement is to find a sufficient large area with uniform terrain characteristics to get reasonable repeatable measurements. Since both Bevameter measurements and vehicle experiments are likely to affect the terrain properties, either the area must be large enough to make it possible to divide it into smaller parts such that each experiment is performed on fresh terrain, or it has to be possible to restore the terrain between each experiment.

For the measurements presented in this thesis, a sand bed with the dimensions $30 \times 5.5 \times 0.6$ m^3 containing uniform sand is used and the sand is restored between the experiments. In practice this was implemented by the following procedure:

1. The sand bed is raked over to even out bumps and holes.
2. A vibrating plate compactor makes the sand compact.
3. The sand bed is gently raked over again in order to get a smooth surface.
4. The test vehicle is run on the bed measuring slip, drawbar pull and wheel torques.
5. Bevameter measurements are performed both in wheel traces and outside the wheel traces where the sand still is prepared.

During night, the sand bed was covered and kept dry by a dehumidifier. The six-wheeled vehicle was braked by a towed vehicle connected by flexible climbing ropes in order to avoid jerks and to get a smooth increasing braking force as the towed vehicle is braking. The drawbar pull is then measured by a force sensor connected to the ropes. In order to be able to calculate the tyre slip and wheel torques, the real vehicle velocity is measured by a trailing measuring wheel and the wheel speeds and hub motor powers are logged from the electric transmission during the tests.

Since the tyre/terrain models uses terrain parameters such as pressure–sinkage and shear stress–displacement relationships, the sand properties are measured with a Bevameter [25]. Parameters in the pressure–sinkage relationships proposed both by Bekker [26] and Reece [27] are estimated to fit the measured data. Both external and internal shearing properties of the sand are measured using a rubber coated shear ring and a shear ring with grousers, respectively, as described in [25].

4.3.1 Bevameter for measuring terrain values

The Bevameter is used both for measuring pressure–sinkage relationships and shear stress–displacement relationships. A drawing of the Bevameter is shown in Figure 4.1. For further description see [25].

A hydraulic cylinder (pos. 2) is used for applying ground pressure. When measuring pressure–sinkage relationships, a plate is mounted at the bottom of

the shaft (pos. 1) that runs through both ends of the hydraulic cylinder and is pressed down into the terrain. Since the plate radius is included both in Bekker's and Reece's equations, at least two plates with different radii have to be used in order to be able to identify all parameters in the equations. The sinkage is measured by a position sensor on the shaft of the hydraulic cylinder.

In this case the Bevameter is mounted on a wheel loader and to eliminate the influence of the flexibility, e.g. in the tyres, a position sensor is also measuring the distance from the hydraulic cylinder to the ground. The ground force is measured by a strain gauge (pos. 3), and since the area of the sinkage plate is known, the ground pressure can be calculated.

To measure shearing, a shearing head (pos. 4) is mounted instead of the sinkage plate on the Bevameter. There are two shearing rings, one rubber covered for external shearing and one in metal with grousers for internal shearing. When measuring shearing, a ground pressure is applied with the cylinder and the cylinder shaft is rotated by a hydraulic motor with a planetary gear (pos. 5).

The guide rail (pos. 6) allows the hydraulic motor housing to move up and down with the piston rod, but prevents it from rotating. The hydraulic cylinders and parallel bars (pos. 7, 8, 9, 10) are used for adjusting the height and storing the Bevameter when it is mounted on the articulated tracked vehicle Bv206. As the Bevameter is mounted on a wheel loader during the measurements described in this thesis, these cylinders are not active. Both the rotational angle and the torque were measured, making it possible to calculate shearing displacement and shear stress since the shearing ring radius and area are known.

Measurements were performed both on the prepared surface, which is the sand the front wheels are rolling on, and in the wheel traces to get the characteristics of the sand beneath the following wheels.

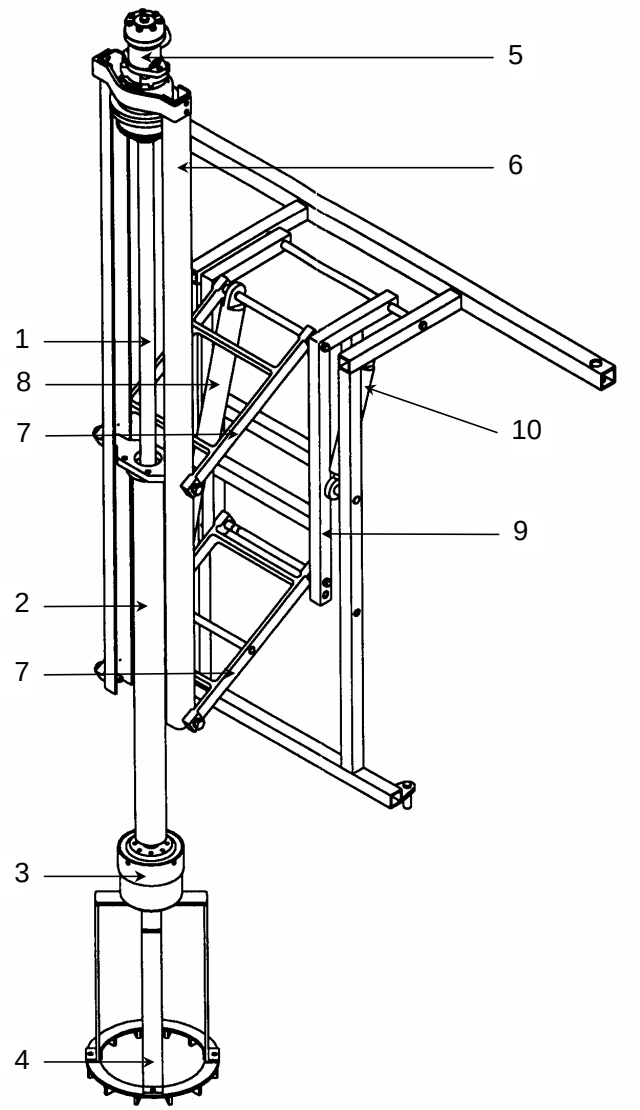

Figure 4.1: Drawing of Bevameter used for measurements.

Chapter 5

Results

5.1 Studied cases

Here, a summary of results describing different aspects of the dynamic performance of six-wheeled vehicles both on- and off-road is presented. The purpose of the studies is to use and evaluate the steering models developed to find out how to steer a six-wheeled vehicle in an appropriate way, use the electric transmission model to evaluate the performance and robustness to faults in the system and to make sure that it is possible to do dynamic simulations both on- and off-road including steering manoeuvres using the developed tyre/terrain models. Since the steering characteristics is important both at high and low speeds and the vehicle usually only drives fast on roads, tyre models for rigid ground were used during the steering simulations. When evaluating the performance of the electric transmission the steering is not important and therefore a simplified vehicle model is possible to use in order to get faster simulations.

The following three different cases have been studied:

- Steering on flat, rigid ground
- Straight forward driving using electric transmission on flat, rigid ground
- Driving on flat, soft ground.

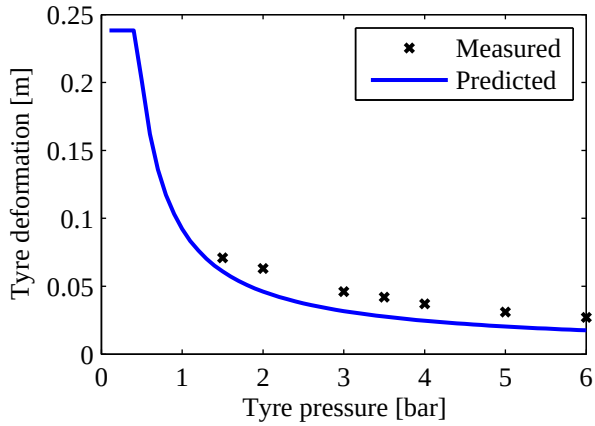

Figure 5.1: Deformation for a tyre on flat, rigid ground.

5.2 Tyre deformation on flat, rigid ground

To evaluate the deformation of the pneumatic tyre model, developed in *Paper E* and also described in Chapter 3.4.4, the tyre is positioned on a flat, rigid surface. As can be seen in Figure 5.1, the measured deformation is larger than the simulated deformation. Contributing to that is probably the simplification in the model that only the sidewalls are deformable, while also the tread part is deformable on the actual tyre.

The brush tyre model described in *Paper F* and Chapter 3.4.2 has an assumption for the pressure distribution, defined in Equation 3.1, which makes it possible to compare to the pressure distribution for the pneumatic tyre model. Figure 5.2 shows that the pneumatic tyre model predicts a more even pressure distribution than the assumption for the brush model.

5.3 Steering strategies

In order to evaluate different steering methods, J-turns are considered to be relevant manoeuvres. In this way information is found about the transient behaviour at the start of the J-turn and also the turning diameter by examining the complete turning path. A steering strategy fulfilling the different demands for both high-speed and low-speed behaviour is then defined by combining different steering methods.

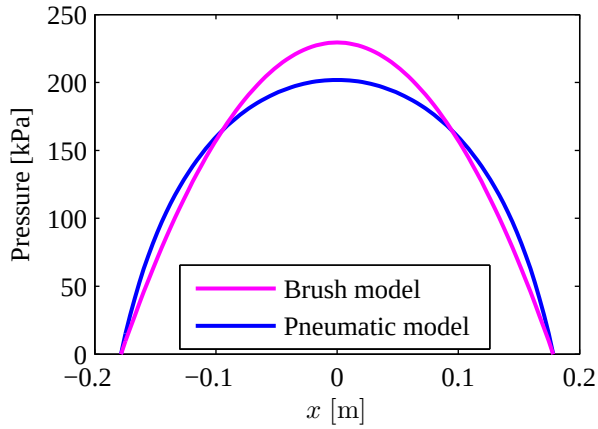

Figure 5.2: Different models for longitudinal pressure distribution in the contact area.

5.3.1 J-turn at constant speed

Paths resulting from the J-turn are shown in Figure 5.3. The dashed line (c) corresponds to front wheel steering alone, the dotted line (b) is used for steering on both front and middle wheels, while the solid line (a) shows the path when rear wheel steering is used together with front wheel steering. It can be seen that method (a) gives the shortest turning diameter as expected, while the largest turning diameter is achieved for method (b).

The fact that steering method (c) will give a shorter turning diameter than when using method (b) might be a bit surprising. Consider using steering method (c) while running the vehicle on only the front and rear wheels. Since the turning centre will be on a line perpendicular to the rear wheels, the turning diameter will be close to when using steering method (b). If we instead run the vehicle on only front and intermediate wheels, the turning diameter will be close to the turning diameter when using steering method (a), since the turning centre in that case is on a line perpendicular to the intermediate wheels. However, if we instead could run the vehicle only on the intermediate and rear wheels, the vehicle would run straight ahead when using steering method (c). When the location of the centre of gravity is in front of the middle wheels, the vehicle will act a little bit more like when running only on the front and middle wheels. Hence, the actual turning diameter depends on where the centre of gravity is located.

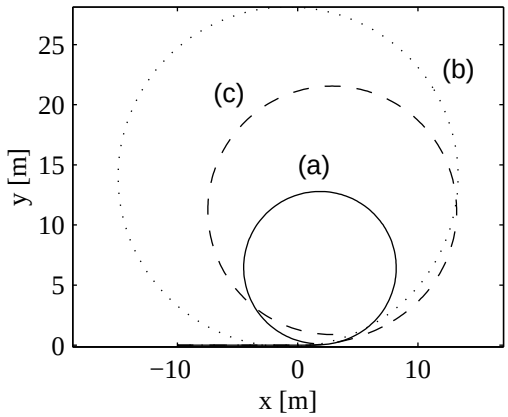

Figure 5.3: J-turn turning paths with the three different steering methods (a) front and rear, (b) front and middle and (c) only front wheels.

5.3.2 Combining steering methods for good performance both at high and low velocities

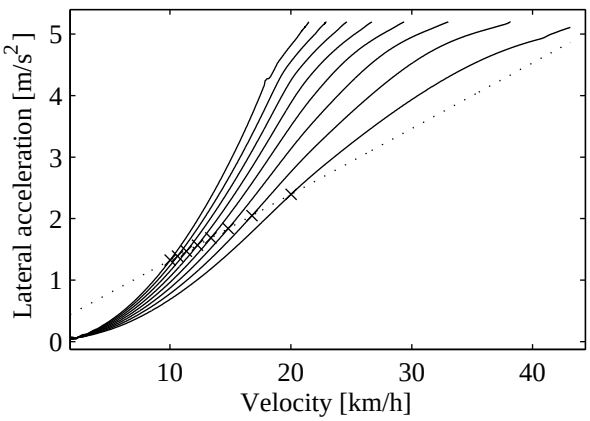

Figure 5.4: Lateral acceleration for 20° steering angle on the front wheels and different steering angles on the rear wheels.

The three different steering methods evaluated and discussed in Chapter 5.3.1 have different characteristics, but when considering both driving at high and low velocities, there is no clear winner. Method (a) is the best choice when driving at low velocity, but the vehicle will not be as stable as it could be at high speeds due to the high yaw rate and slow lateral response. More reasons to avoid method (a) at high velocities are the risk of overturning and that the

method probably is bad in case of skidding since the slip angle for the rear wheels will increase when counter-steering. Since the small turning diameter cannot be used at high velocities, a combination of two different methods such that method (a) is used at low velocities and (b) or (c) at high velocities would be good. Considering only steering performance, method (b) seems to be the best choice. However, method (c) is not far from the same performance, but requires no steering actuator on the intermediate wheels and thus no space consuming wheel housings for steering. Thereby, a combination of method (a) and (c) is suggested. In order to make the vehicle easy and safe to drive, the transition between the two methods should be automatic and smooth. The transition can be performed both by reducing the maximum allowed steering angle for the rear wheels as the velocity increases and keeping the same steering angle on the rear wheels as on the front wheels up to that maximum allowed angle, or by reducing the gain such that the rear wheels steering angle is a smaller part of the front wheels steering angle as the velocity increases. Since just reducing the maximum allowed steering angle for the rear wheels as the velocity increases will lead to a highly non-linear response to the steering wheel when that angle is reached, only reducing the gain are considered here. The non-linear response would probably be felt inconvenient to the driver, and could also result in dangerous driver-vehicle behaviour.

The solid lines in Figure 5.4 show the lateral acceleration with a steering angle of 20° on the front wheels. The rear wheel steering angle is 20° for the left curve, 18° for the next one and reduced in steps of 3° down to 0° for the right curve, i.e. the left curve represents steering method (a) and the right curve represents steering method (c). Since the lateral acceleration is increasing with speed, the lateral acceleration should be increasing with speed also during the transition in order to get a smooth transition from (a) to (c). The dotted line shows a linear increase of the lateral acceleration. By following that line during the transition, the vehicle will use method (a) up to 10 km/h and method (c) over 20 km/h.

More details on how to determine appropriate rear wheel steering angle and results are presented in *Paper A*.

5.4 Pivot turn

The model described in *Paper F* has also been used to evaluate pivot turning times. Measured and simulated pivot turning times at different power consumptions are shown in Figure 5.5. The largest uncertainty in the measurements is

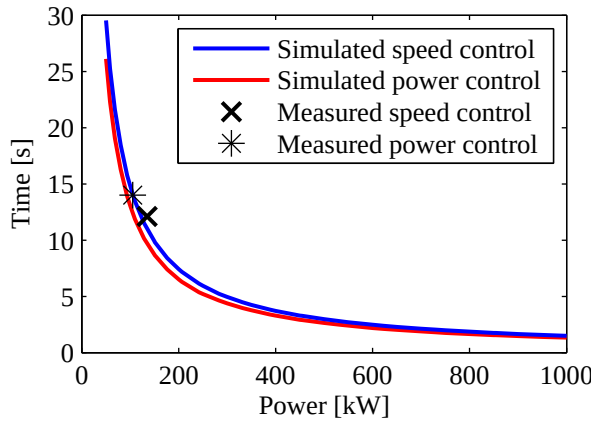

Figure 5.5: Pivot turning time is depending on available power.

the mechanical power on the wheels, since it is hard to measure without measurement rims. During the measurement for speed control, the power consumption of the wheel hub motors is measured. Since that measurement was not possible to do during the power control measurement, the diesel engine power is used instead. The estimated power loss is subtracted from the measurement in order to show the mechanical power on the wheels in Figure 5.5. The simulation results agrees reasonably well with the measured values, but it seems like the actual power demand is slightly higher in reality than the model predicts. The largest uncertainties contributing to that are probably the efficiency of the electric transmission and the coefficient of friction.

By running the middle wheels slower than the corner wheels, it is possible to achieve a faster pivot turn, which is shown in Figure 5.6, where the power is kept at 200 kW. The optimal speed on the middle wheels is 60 % of the speed on the corner wheels. By controlling all the hub motors to the same power, the speed on the middle wheels becomes close to the optimal speed.

An efficient method to reduce the pivot turning time is to reduce the load on the corner wheels, which is shown in Figure 5.7. However, it is likely to take some time to adjust the load distribution, depending on the suspension system.

By changing the control strategy and the load distribution, it is possible to affect the energy dissipated during the pivot turn shown in Figure 5.8. The simulations are performed with 200 kW available power, but the result is independent of the power. As more load is distributed to the middle axle, the energy consumption is reduced. At the same time, the benefit of reducing the speed on the middle axle is also reduced.

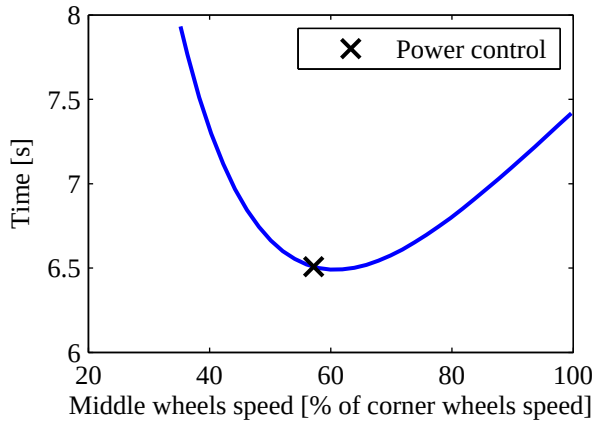

Figure 5.6: Keeping the total power consumption constant, the middle wheels should be run slower than the corner wheels to minimise the pivot turning time.

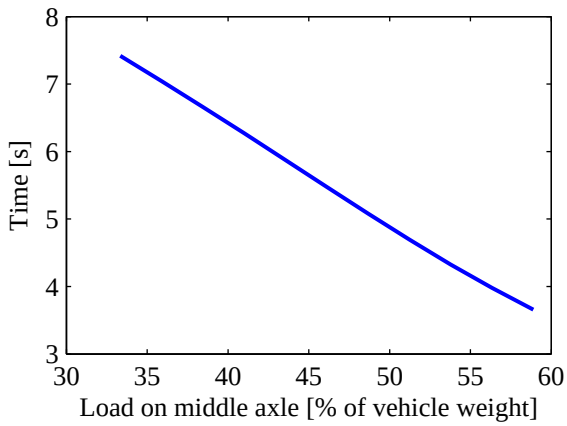

Figure 5.7: The pivot turning time is reduced when more load is distributed to the middle wheels.

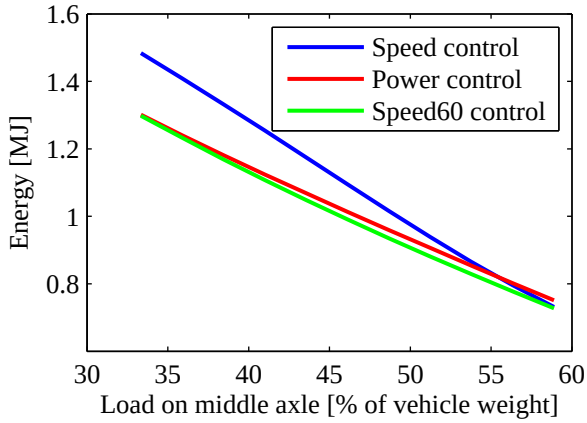

Figure 5.8: The pivot turning time is reduced when more load is distributed to the middle wheels.

5.5 At-the-limit handling

Only a summary of improving at-the-limit handling is given here. See *Paper F* for more details.

5.5.1 Steering methods

Since steering can be achieved both by applying steering angles and torques on the wheels, several different configurations are possible. It has been shown that by combining front wheel steering with rear wheel steering it is possible to achieve good steering performance at both high and low speed [28] without the need for large steering angles on high friction roads.

Here, the performance of such a vehicle is evaluated on low friction surfaces and compared to a more conventional vehicle with larger steering angles on the front wheels. To find out if it is possible to improve the performance by using individually controllable wheel torques, a vehicle with front wheel steering and individually controllable wheel torques is included. In total, four different vehicle configurations are evaluated:

- FWS: Front wheel steering with a maximum steering angle of 20°.
- FMWS: Front and middle wheel steering with a maximum steering angle of 30° on the front wheels and 15° on the middle wheels.

- FRWS: Front and rear wheel steering with a maximum steering angle of 20° on both front and rear wheels.
- FWS+TC: FWS combined with individual wheel torque control.

For FMWS and FRWS, the applied steering angle on the middle and rear axle, respectively, is proportional to the steering angle on the front wheels. The steering angle on the middle axle is set to half the steering angle on the front axle.

For the rear axle, the optimal steering angle is not known in advance. Therefore, the performance for FRWS in each manoeuvre is evaluated for different rear axle steering angles, and the results for the best performing rear axle steering angles are shown in the plots. To implement a general controller for FRWS, it might be necessary to take more variables than front axle steering angle and vehicle velocity into account, although the initial assumption is that the rear axle steering angle is proportional to the front axle steering angle during the evaluated manoeuvres.

FWS+TC uses β feedback control of the wheel torques. The choice of this more advanced controller is made since there is no obvious mapping from front axle steering angle to wheel torques and, as will be shown, the torque distribution to achieve the desired yaw torque is depending on β. During dynamic simulations, the more advanced controller is unfair to the other steering methods, since it has a stabilising effect on the vehicle. However, this fact will be taken into account during the evaluation, and most of the simulations will be performed in steady state.

5.5.2 Comparison of steering methods and individual wheel torque control

5.5.2.1 J-turn

To evaluate the J-turn performance, CG traces of the vehicles are analysed. The driver is initially driving straight ahead along the X-axis, and starts turning the steering wheel at $(0, 0)$. At a certain X position, the corresponding Y position is measured and compared between the different steering methods. The vehicle velocity is initially 90 km/h, but no velocity controller is applied, which implies that the velocity will decrease during the manoeuvre.

Controlling the wheel torque does not increase the lateral force much, but as the vehicle slip angle increases, the centripetal force also increases and the vehicle

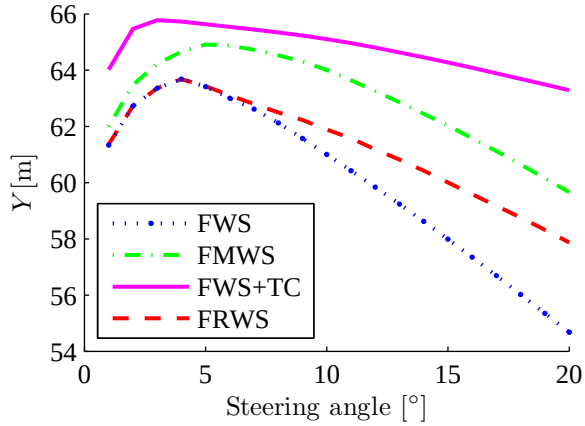

Figure 5.9: Y position at $X = 300$ m vs. steering angle during a J-turn for different vehicle steering configurations and $\mu_s = 0.1$.

steering performance is improved, as shown in Figure 5.9. Since the vehicle is running on a low friction surface, there is an optimal steering angle, for which the vehicle turns as much as possible.

By controlling the wheel torques, it is possible to decrease the sensitivity for too large steering angles and maintain a reasonable steering performance although the steering angle is larger than the optimal steering angle. By using FWS+TC it is possible to exceed the steering performance of FMWS at $X = 300$ m.

As can be seen in Figure 5.9, the steering performance is improved compared to FWS for large front wheel steering angles as the small rear wheel steering angle is applied, but does not reach the performance of FMWS or FWS+TC.

5.5.2.2 Rear wheel skid

During a rear wheel skid, the driver might be able to achieve an aligning torque by steering into the skid and thereby gain control over the vehicle again. In this evaluation, the vehicle slip angle is set to $\beta = 25°$. The maximum steering angle is assumed to be limited to $20°$ for all steering methods except FMWS, but the evaluation is done for $\delta_{1,2} \leq 30°$ for all steering methods anyway.

At $\mu_s = 0.3$, the power limit of the wheel hub motors is reached for $\delta_{1,2} > 15°$, i.e. when the front wheels are close to, but not entirely, aligned to the direction of travel, thus increasing the power demand to affect the lateral force.

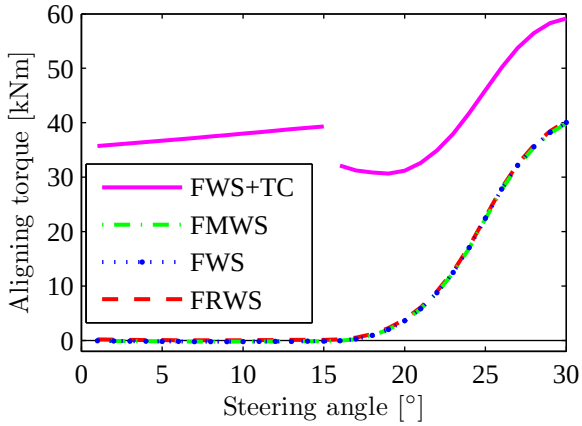

Figure 5.10: Aligning yaw torque for different steering methods, $\beta = 25°$ and $\mu_s = 0.3$.

In Figure 5.10, a discontinuity is seen in the aligning torque for FWS+TC as the power limit is reached.

Although the power limit is reached, the aligning torque is vastly improved, making it possible to achieve a reasonable aligning torque even if the front wheel steering angle is limited to $|\delta_{1,2}| \leq 20°$. FWS, FMWS and FRWS all have similar performance, but the front wheel steering angle has to exceed 20° for these steering methods in order to achieve a reasonable aligning torque.

5.6 Driving using electric transmission

The focus in *Paper B* is simulation models for the electric transmission. The simulated vehicle is assumed to have two diesel engines with generators and six wheels with hub motors. For simplicity only one diesel engine, one generator and one drive motor is simulated. The power consumed by the drive motor is multiplied by 3 in order to get a realistic load on the generator and diesel engine and the force produced by the drive motor is multiplied by 6 to get a realistic simulation of the vehicle acceleration. The diesel engine has an inner friction in order to make it possible to dissipate power, but apart from that no losses are simulated, which means that the performance will be better in the simulations than what can be expected in reality.

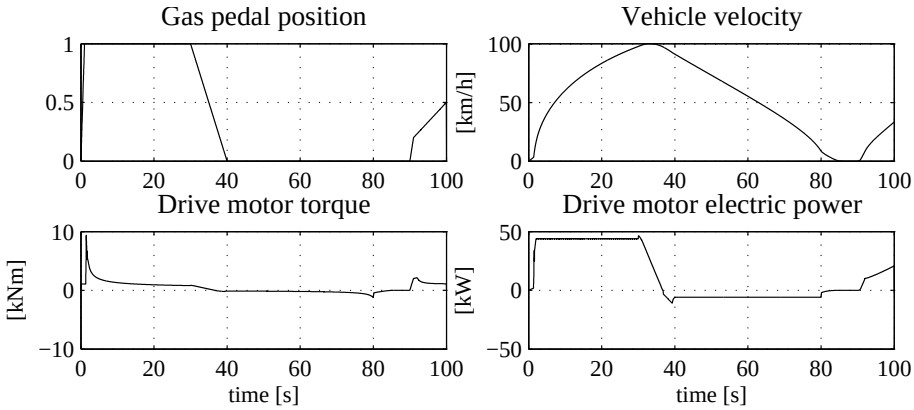

Figure 5.11: Gas pedal position (1 corresponds to full gas, 0 is released gas pedal), vehicle velocity, drive motor torque and drive motor electric power.

5.6.1 Acceleration and braking

Simulation results for a simulation with full acceleration, motor braking and a short slow acceleration part are shown in Figure 5.11. When the accelerator pedal is pressed, the diesel engine speed set point is increased by the powertrain main controller and the diesel engine speed controller sets full throttle to increase the speed. In the simulation, the accelerator pedal is pressed before the DC bus is charged and the generator controller will not charge the DC bus until the diesel engine has reached the desired speed. The powertrain main controller also sets a high torque command to the drive motor as the accelerator pedal is pressed, but the drive motor will not produce full torque until the DC bus is charged. This means that there is a delay before the drive motors will produce full torque when the accelerator pedal is pressed, and this delay is depending on the diesel engine dynamics.

During the acceleration, the drive motor is limited by the maximum power and the torque gets lower as the speed increases. After 30 s the vehicle has accelerated to 100 km/h and the accelerator pedal is released. When the accelerator pedal is released and the vehicle is running, the drive motor will brake electrically in order to mimic engine braking on cars with mechanic transmissions. However, the torque is low since only a limited amount of power can be dissipated to the diesel engine. In order to keep the DC bus voltage within range, the drive motor controller moderates the braking torque when the DC bus voltage is high. The generator controller tries to keep the voltage down by driving the diesel engine, but only a limited amount of power can be dissipated without

overspeeding since the braking torque of the diesel engine is lower than what can be provided when driving. The diesel engine is running at high speed when braking, but it is not consuming any fuel since the engine throttle is 0. When the vehicle stops after a little bit more than 80 s, no more power is dissipated. The electric power both on the generator and the drive motor is 0, and the engine throttle is increased in order to prevent the diesel engine from stalling and keep the idle speed.

After 90 s the accelerator pedal position is increased such that the diesel engine speeds up and the vehicle starts moving again. Now the maximum power at the diesel engine speed set point is higher than the power needed by the drive motors and thus the engine throttle position will not be at maximum.

5.6.2 Driving with reduced diesel engine performance

It is important that the control system is robust to reduced diesel engine performance in order to make it possible to drive e.g. in case of turbo charger failure. When the performance is reduced there is a risk that the maximum power the diesel engine can deliver at the speed set point calculated from engine maps by the powertrain main controller is lower than the demanded power. If the generator puts too much load on the diesel engine, the speed will go down and the maximum power it can deliver will be reduced even more. Eventually the engine will stall if the generator power is not reduced.

In the simulation, the diesel engine maximum power is reduced to be one half of the normal power above 2000 r/min.

In order to handle that situation, the generator controller reduces the power to the DC bus if the diesel engine speed deviates too much from the set point. Thus, the DC bus voltage will drop and the drive motor has to reduce the power output in order to keep the DC bus voltage. Now the vehicle only reaches about 60 km/h, which can be seen in Figure 5.12. Electrical braking works as good as in the previous simulation since the possibility to dissipate power is not affected. During the slow acceleration at the end of the simulation starting at 90 s, the diesel engine throttle is at maximum since the speed set point is too low to make it possible to produce the desired power.

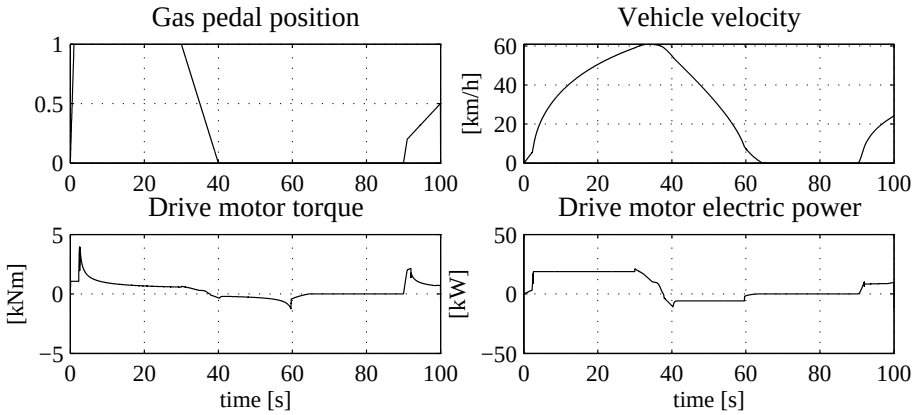

Figure 5.12: Gas pedal position (1 corresponds to full gas, 0 is released gas pedal), vehicle velocity, drive motor torque and drive motor electric power with reduced performance on diesel engine.

5.7 Driving on soft ground

When evaluating the developed tyre/terrain model, the vehicle is chosen to be run in a circle, according to Figure 5.13. A speed controller is used to determine the torque of the wheels and the same torque is applied on all wheels. Parts of the simulation results presented in *Paper C* are shown for the case when the vehicle is run with the same steering angles, but with individual speed controllers for each wheel. In that case the torques of the inner wheels will be higher than on the outer wheels, which will counteract the steering and the circle will have a larger diameter as is shown in Figure 5.14.

5.8 Pressure–sinkage relationships

5.8.1 Measurements on sand

To measure the pressure–sinkage relationship on compact sand, measurements are performed with two different plates with diameters 100 mm and 150 mm, respectively. Measured sinkage and pressure for prepared sand is shown in Figure 5.15. The adapted models are based on data down to 0.14 m. There are several reasons for not using all data for estimating the models. The larger the sinkage plates are, the larger the force is needed for pushing it down, but the force the Bevameter can provide is limited, which in turn constrains the

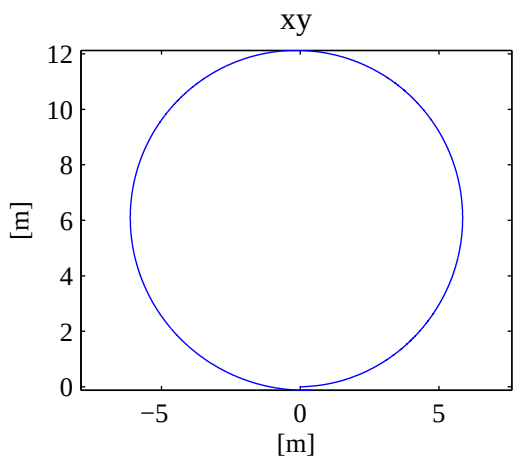

Figure 5.13: Vehicle path when turning on soft ground using both front and rear wheel steering and equal torque on all wheels.

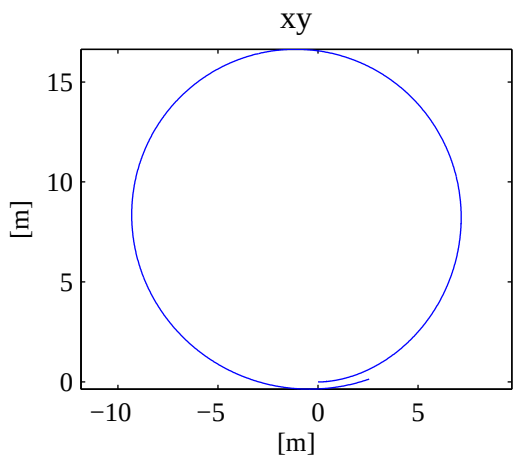

Figure 5.14: Vehicle path when turning on soft ground using both front and rear wheel steering. The torque of the wheels are determined by a speed controller.

achievable depth. As a consequence, data is only available for the smallest sinkage plate at the largest sinkages. If the vehicle sinks down too much, it will get stuck. Thus, it is not practically possible to run the vehicle with large sinkages and measure drawbar pull. Therefore, the terrain properties at large sinkages will not be useful for validation of the tyre/terrain interaction model later on. As the sinkage increases, the sinkage plate will come closer and closer to the concrete below the sand bed, and phenomenons that are not existing close to the surface where the vehicle is run might be measured. By limiting the data to the relevant region, the models will be best adapted to the conditions under which they will be used during the tyre/terrain model validation.

Both Equations 3.2 and 3.3 have been adapted to the measured data. Since the specific weight, γ, and cohesion, c, are needed in Equation 3.3, the specific weight is measured by using a measuring cup and a scale. No effort was made to try to resemble the exact compactness of the sand in the sand bed when measuring it in the measuring cup, or to identify a difference in specific weight between compact and loose sand. Although the measured value will affect the estimated terrain value k'_ϕ, it has no influence on the predictions since it is the product $\gamma b k'_\phi$ that is used in the model.

The predictions from Equations 3.2 and 3.3 coincide, which is shown in Figure 5.15.

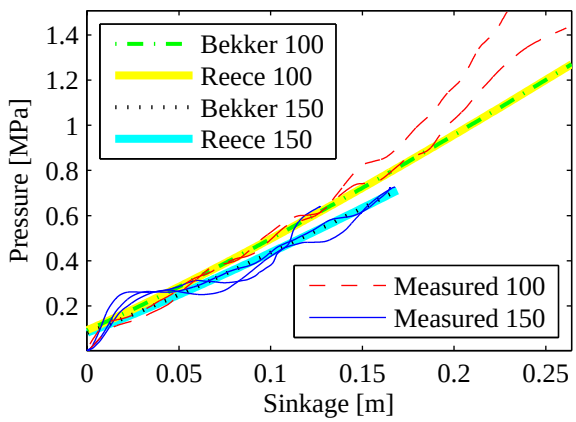

Figure 5.15: Measured pressure and sinkage on compact sand. All measured data are shown in the figure, but the estimated models are based on sinkages down to 0.14 m.

The sand properties in the wheel traces are depending on the wheel slip. In wheel traces where the test vehicle has been driven with low slip, no differences from the prepared sand was seen in measurements. The prepared sand bed is

already compact and, except from the visible wheel traces on the sand bed, the effect on the sand of running the vehicle with low slip is negligible. As the slip increases, the wheels start to move sand and let it settle behind the wheels without compacting it, creating a layer of loose sand in the upper part of the wheel trace. The thickness of the loose sand layer is increased with higher tyre slip and deeper wheel sinkage. On loose sand in high slip wheel traces, measurements are performed with three different plates with diameters 100 mm, 150 mm and 200 mm, respectively. Measured sinkage and pressure for loose sand is shown in Figure 5.16. As in the measurements on prepared sand, the adapted model is based on data down to 0.14 m.

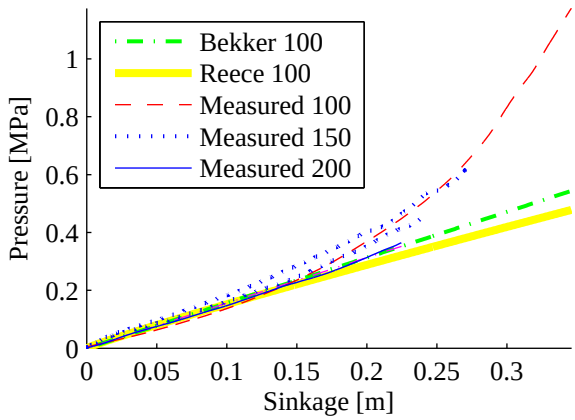

Figure 5.16: Measured pressure and sinkage on loose sand. All measured data are shown in the figure, but the estimated models are based on sinkages down to 0.14 m. Predictions are only shown for the smallest sinkage plate since the predictions for larger sinkage plates coincide and cannot be discerned from the smallest sinkage plate.

The model fit for prepared sand, shown in Figure 5.15, is improved by adding an offset to the sinkage such that the model already predicts a pressure as the sinkage plate meets the sand surface. This might be due to the vibrating plate compactor making the sand a bit more compact near the surface. Also, the measurements show a clear increased stiffness near the surface, but the indicated thickness of this possible layer varies significantly with the size of the sinkage plate. When using the larger sinkage plate, the increased stiffness will be maintained further down into the ground than when using the smaller sinkage plate. However, measuring pressure–sinkage relationships is not easy, since sometimes the sand beneath the sinkage plate will form kind of a pole with high stiffness. As that pole breaks, the sand starts moving around the sinkage plate and the sinkage is rapidly increased without affecting the ground pressure

much. This phenomenon makes the measurements irregular and might contribute to the measurements showing a higher stiffness near the surface. Still, since the model adaptation is best when considering an offset on the sinkage, it seems likely that the vibrating plate compactor is affecting the sand close to the surface by making it a bit more compact. The measurements on loose sand, which is not affected by the vibrating plate compactor, does not show any increased stiffness at the surface, but at the same time the loose sand is not exposed to the phenomenon of making poles either, which makes these measurements much smoother. Since it is the high slips of the tyres that made the layer of loose sand in the wheel traces, the sand closer to the bottom of the sand bed will still be compact, and a significant increase in the stiffness is shown in the measurements at high sinkages. Also the measurements on prepared sand have a tendency of showing increased stiffness at high sinkages. There are at least two things that might contribute to that. The sand close to the bottom of the sand bed is hardly ever exposed to high wheel slip, which might have made this sand more compact than the sand closer to the surface that is sometimes moved around. At the same time, the closeness to the bottom of the bed might make the pole phenomenon appear more easily there, since the floor below the sand bed is rigid concrete.

5.9 Shear stress–displacement relationship

To establish the shear stress–displacement relationship, measurements are performed with two different shear rings on the Bevameter, one rubber coated to measure external shearing and one with grousers to measure internal shearing. The model for shear stress–displacement in Equation 3.9 can be rewritten as

$$\tau = \tau_{max}\left(1 - e^{-j/K}\right), \tag{5.1}$$

where

$$\tau_{max} = c + \sigma \tan\phi. \tag{5.2}$$

That is, τ_{max} is, according to the model, a linear function of σ. Therefore, shear measurements are performed at several different ground pressures and the terrain values c and ϕ are estimated by a least squares fit. The measured maximum shear stresses at different ground pressures are shown in Figure 5.17 together with the least squares fit. The identified terrain values are shown in Table 5.1.

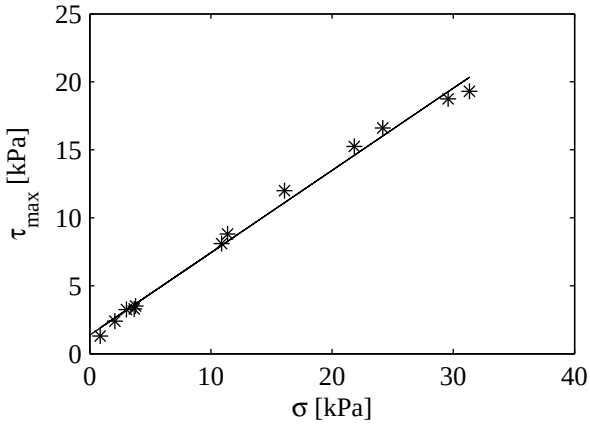

Figure 5.17: Measured maximum shear stress at different ground pressures (*) and a least squares fit (-).

Table 5.1: Measured terrain values.

Terrain values		Compact	Loose
K	m	0.047	0.074
k_c	kN/m^{n+1}	95.7	0
k'_c		24.5	0
k_ϕ	kN/m^{n+2}	3277	1585
k'_ϕ		185.1	112.3
n		1.15	1.01
n'		1.15	0.924
c	kPa	1.37	1.57
γ	kN/m^3	14.2	14.2
ϕ	°	31	37

To estimate the shear deformation modulus, K, the shear stresses are normalised by dividing by the maximum shear stress. Then the model

$$\frac{\tau}{\tau_{max}} = \left(1 - e^{-j/K}\right) \tag{5.3}$$

is adapted to the measured data by minimising the root mean square error with the Nelder-Mead simplex method. The measured shear stress–displacement relationships and the estimated model are shown in Figure 5.18 and the estimated shear deformation modulus is also shown in Table 5.1.

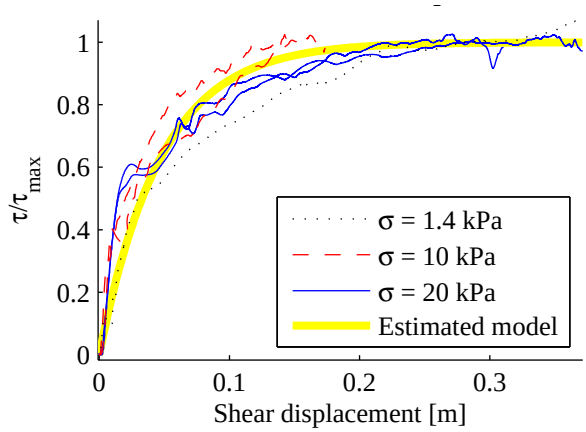

Figure 5.18: Measured maximum shear stress at different ground pressures and a least squares fit model.

5.10 Drawbar pull on sand

To compare the measured and simulated drawbar pull, the contribution from one wheel at different tyre pressures is shown in Figure 5.19. The predictions agree reasonably well with the measurements at 1.5 bar and 3 bar, but at 5 bar the prediction vastly exceeds the drawbar pull measured with the vehicle. Actually, the vehicle was barely able to run on the sand bed with 5 bar pressure in the tyres. Also the predictions for rigid tyres exceeds the measurements at 5 bar.

Since the prepared sand was easier to walk on than the loose sand exposed to high slip in the tracks, it initially seemed likely that one reason could be that only the front wheels are running on the prepared sand, while all the remaining

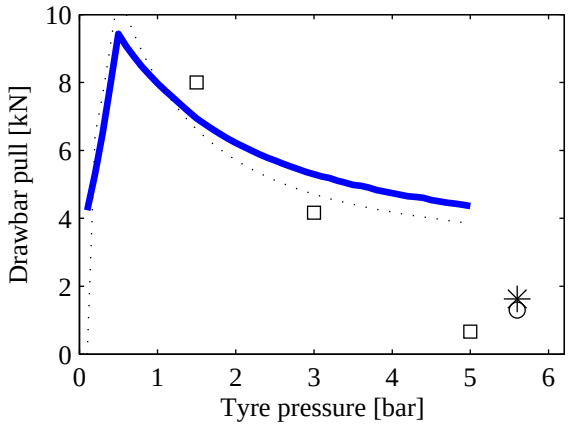

Figure 5.19: Simulated drawbar pull on prepared sand bed (—) at varying tyre pressure. Simulated drawbar pull on loose sand (· · ·), measured drawbar pull (□) and simulated drawbar pull for a rigid wheel on prepared sand (○) and loose sand (∗) are also shown.

wheels are running in the ruts. However, as can be seen in Figure 5.15, the pressure in the prepared sand is increased more for smaller sinkage plates, and the tyres are significantly wider than the smaller sinkage plates. Predictions for tyres on loose sand are included in Figure 5.19 and show that the drawbar pull only differ slightly from the predictions for tyres on prepared sand.

A probable cause of the diverging result at high tyre pressure is that the tyre tread bulges out in the centre forming a crowned shape, which increases the lateral stresses and decreases the vertical force from the normal stresses.

The tyre sinkage is thus increased, giving higher rolling resistance and thereby decreasing the drawbar pull. The increased lateral stresses will also contribute to the three-dimensional behaviour of the soil failure described by Karafiath [29] and Wiendieck [30]. Thus, the real tyres will get lower ground pressure beneath the tyre and will perform worse than the predictions, since the model assumes the tread to be rigid in the lateral direction and neglects the lateral stresses when determining θ_m.

As the tyre tread gets more crowned when the tyre pressure is increased, the model deviates more from the actual tyres at higher pressure.

Assuming that the tyres are not deformed at high tyre pressures, as proposed for example in [21], would improve the predictions at 5 bar, but it would be hard to determine the transition from rigid to flexible tyre. Figure 5.20 show that the normal stresses never exceeds 2.5 bar for a rigid wheel during the cir-

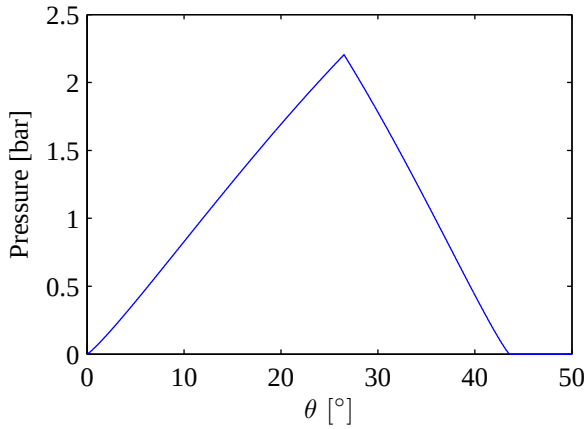

Figure 5.20: Normal stresses beneath a rigid wheel with 2250 kg vertical load at 30 % slip.

cumstances in the measurements, while the performance is vastly improved by lowering the tyre pressure from 5 bar to 3.5 bar as can be seen in Figure 5.19. That is, the tyres seem to be deformed although the normal stresses from the sand is lower than the tyre pressure, which is also predicted by the radial tyre deformation model shown in Figure 3.14.

A critical analysis of why the pressure–sinkage and shear–displacements relationships approach might give bad predictions for vehicle–terrain interaction performance is given in [31], where it is argued that relationships such as Equations 3.2 and 3.9 only are relevant to a particular test setup and can be totally misleading if they are applied to tyre/terrain interaction models. It is obviously true that the geometry is different between measuring terrain values with a Bevameter and rolling a wheel over soft ground. From the measurements in this thesis, its seems that the Bevameter measurements contain relevant information to predict drawbar pull, at least on dry sand. However, at low tyre pressures the geometry in the tyre/soil interface is rather close to the geometry in the Bevameter measurements, but the higher the tyre pressure is, the more the geometry in the tyre/soil interface deviates from the geometry during the Bevameter measurements. Thus, the difference in the geometry might be contributing to the deviation between predicted and measured drawbar pull at 5 bar.

Chapter 6

Discussion of appended papers

6.1 Paper A — Six wheeled vehicle steering

The aim of the work presented in this paper was to evaluate different steering methods for six-wheeled vehicles and preferably find a steering method that does not need large wheel housing, uses few actuators, gives a small turning diameter at low speed and fulfils the Ackermann steering geometry, at least at low velocities.

The presented vehicle model of 15 degrees of freedom can predict the main steering characteristics for six-wheeled vehicles. It has the advantage that during development of vehicle controllers the simulations start quickly giving a fast feedback indicating if the controller works. When the controllers work satisfactorily well, the simple vehicle model can be exchanged for a slower but more accurate vehicle model developed in ADAMS.

The coefficient of understeering can be derived from the equations of motion for six-wheeled vehicles, but if it is done for small angles the predictions are not relevant for large steering angles.

At low velocities steering on both front and rear wheels gives a short turning diameter with small steering angles and thereby also small wheel housings. Steering on both front and intermediate wheels gives best performance at high velocities, but steering only on the front wheels is almost as good. By controlling the rear wheel steering such that the rear steering angle is reduced as

the velocity increases, it is shown that it is possible to realise a steering system with only two actuators, small wheel housings and acceptable performance both at high and low velocities.

6.2 Paper B — Simulation of electric transmission

The aim of the work presented in this paper was to develop simulation models for an electric transmission, that can be used in vehicle dynamics simulations to get physically reasonable bounds for what is possible to achieve from the electric transmission.

The powertrain demands for a six-wheeled off-road vehicle are modelled, analysed and the desired characteristics of the drive motors are determined. Since a high torque is desired at low speeds, a gearbox is probably needed for the drive motors. Depending on chosen type of drive motor, a two-step gearbox might be needed.

Simplified models for components in the electric transmission are developed, which makes it possible to simulate and analyse the control architecture. A straightforward and robust control layout is suggested.

Simulations show that the proposed control architecture can control the electric transmission. Even if the diesel engine performance is reduced the controllers will let it speed up in order to produce as much power as possible.

The simulated control strategy is not optimised for keeping the DC voltage constant. On the other hand, it is robust and can handle uncontrolled loads on the bus. Alternative control strategies are possible and there are methods that are better suited if it is necessary to minimise the voltage variations on the DC bus.

6.3 Paper C — Tyre and terrain models

The purpose of the terrain models presented here is to be used for dynamic simulation of vehicle behaviour. It is also desired to be able to validate the models by experiments. To get reasonable simulation times the models should not include complicated calculations, such as when using the finite element method (FEM). Another important aspect is that it should be possible to measure the terrain parameters where it is possible to drive a vehicle. The derived model presented in here fulfils these demands.

It is possible to measure the terrain values needed for the pressure–sinkage relationship and for the shear stresses by using the Bevameter technique. However, additional parameters are needed in order to predict the point of maximum pressure on the wheel. Thereby it is not straightforward how to get all the terrain values needed to make simulations for a terrain where a real vehicle is driven.

6.4 Paper D — Measuring terrain values and drawbar pull

The aim of the work presented in this paper was to get measurements to be able to validate developed tyre/terrain models.

Measurements of both terrain values and vehicle drawbar pull are performed in a sand bed with uniform sand in order to be able to compare simulation results to real data. A Bevameter is used to measure the terrain values to get data for the terrain models. By attaching elastic climbing ropes to the test vehicle and towing another vehicle that is braking more and more, the drawbar pull is measured at three different tyre pressures.

It was found that the drawbar pull was vastly improved by lowering the tyre pressure. The rolling resistance when towing the vehicle was reduced by lowering the tyre pressure.

6.5 Paper E — Pneumatic tyre models and comparing simulated drawbar pull to measurements

The tyre/terrain models developed in *Paper C* are further developed to include pneumatic tyres. To determine the shape of the tyre/terrain interface, a model for the tyre sidewalls is used to find the equilibrium between the soil and the tyre carcass. Drawbar pull predictions are made with the pneumatic tyre model, and the result is compared to the measured drawbar pull from *Paper D*.

It is shown that the model is suitable for tyre pressures between about 1–4 bar, which is valid for the intended use, i.e. to be able to validate the proposed tyre/terrain models for pneumatic radial tyres that are developed to simulate the behaviour of a six-wheeled vehicle with electric transmission on soft ground. However, at higher tyre pressure, the predicted drawbar pull exceeds the measurements. Even the predictions for a rigid wheel exceeds the measured drawbar

pull at 5 bar. The simplification to only include sand stresses in the vertical longitudinal plane of the tyres is likely to contribute to the deviation at higher tyre pressures, since the lateral sand stresses reduces the ground pressure. Thereby, the sinkage and the rolling resistance are increased and the drawbar pull is decreased.

The simplified tyre deformation model is also using a two dimensional model for the tyre sidewalls. Moreover, the rear end of the tyre/terrain contact area is determined from the maximum tyre deflection, independently from where the point of maximum deflection is located. In that way, the flexible tyre/terrain model becomes identical to the rigid wheel model for infinite high tyre pressure. For low tyre pressures and zero slip, the shape of the tyre/terrain interface is symmetric around a vertical line through the wheel centre in the longitudinal direction. However, at high tyre pressures and high slip conditions, the model is likely to predict a longer tyre/terrain contact area than what is achieved in reality.

Another uncertainty that has huge influence on the predicted drawbar pull is the location of the maximum pressure in the tyre/terrain interface. Since no equipment was available to measure the stresses beneath the tyre during the experiments, a theoretic approach is utilised, where it is assumed that the maximum pressure is located where the principal stress direction is vertical.

However, the proposed model seems to agree well with measurements except at high tyre pressures. From the available measurements, it is not possible to determine if the deviation at high tyre pressures is mainly due to the crowned shape of the tyre, or deficiencies of the model.

6.6 Paper F — At the limit handling

To evaluate the handling characteristics for a six wheeled vehicle during low ground friction conditions, a brush tyre model is developed in order to be able to handle large combined slips. Different manoeuvres are evaluated to find out how the performance is affected by steering method and how individual torque control can improve the performance.

During practical experiments, the drivers found that it was hard to control the six wheeled vehicle with small steering angles both during front and rear wheel skids. The purpose of *Paper F* is to compare the vehicle behaviour during different manoeuvres to find out why the vehicle with small steering angles is harder to control. In particular, it is interesting to find out if the rear wheel

steering system can remedy the inferior performance. Since the vehicle is assumed to be equipped with in-hub electric motors, it is also interesting to find out how individual wheel torque control can improve the behaviour.

The results show that the rear wheel steering system can improve the ability to control the vehicle during a front wheel skid, but not during a rear wheel skid. Individual torque control has the ability to improve the ability to control the vehicle during all the evaluated manoeuvres, i.e. also during rear wheel skids. In the simulations, the controller for the individual torque control included an algorithm to stabilise the vehicle, while the controller for the rear wheel steering was simpler and did not include β-feedback. By including β-feedback control to the rear wheel steering controller it is probably possible to improve the performance for rear wheel steering during some manoeuvres. However, the main drawback of using the rear wheel steering to improve performance during low ground friction conditions remains; it is not possible for the rear wheel steering system to significantly help the driver to control the vehicle during a rear wheel skid. Thus, to improve the performance both during front and rear wheel skids, the maximum steering angle on the front axle has to be increased, or individual torque control is needed.

Chapter 7

Scientific contribution

This chapter lists the main scientific contribution of the thesis and appended papers (listed in chronological order of the work):

1. The development of steering strategies for six-wheeled vehicles in *Paper A*.
2. The development of an electric transmission simulation model appropriate for determining system limitations in vehicle dynamics simulations in *Paper B*.
3. The development of lateral forces for the tyre/terrain interaction model in *Paper C*.
4. The method to perform measurements for comparing simulation results to actual vehicle performance in *Paper D*.
5. The development of a tyre/terrain interaction model for pneumatic tyres on soft ground in *Paper E*.
6. The strategies to improve the at-the-limit handling behaviour for a six-wheeled vehicle in *Paper F*.
7. The strategies to improve pivot turning performance in Chapter 5.4.
8. The proposed modelling environment that enable analysis of the driving dynamic performance of six-wheeled hybrid electric vehicles both on- and off-road, summarising the main content in this thesis.

Chapter 8

Discussion and conclusions

The aim of this work was to identify and implement a suitable modelling environment for analysis of the driving dynamic performance of six-wheeled hybrid electric vehicles both on- and off-road. In this work, vehicle models, including tyre models, for simulating driving on firm ground and terrain models for simulating driving on soft ground have been developed. In addition, models describing the dynamic behaviour of an electric transmission are derived. This makes it possible to simulate the dynamic behaviour of a six-wheeled vehicle both on- and off-road. For rigid ground both models intended for simulating driving during low slip conditions and models capable of simulating large combined slips in a physically reasonable way are included. Models both for rigid wheels and pneumatic radial tyres are developed for simulating driving on soft ground.

Using the models for firm ground, on which it is realistic to drive fast, steering strategies for driving at different velocities are proposed. It is shown that the load distribution due to acceleration, deceleration and the position of the centre of gravity (depending on the carried load) affects the steering properties. Also, the tyres are shown to affect the steering properties, which highlight the importance of relevant tyre data for off-road tyres.

The models intended for large combined slips on rigid ground are utilised both to simulate pivot turning on high ground friction and evaluating at-the-limit handling on low ground friction. Methods for increasing the pivot turning speed are proposed and evaluated in simulations. In the simulations on low ground friction, methods based on rear wheel steering and individual torque control to improve the manoeuvrability are evaluated.

The purpose of the models for the electric transmission is mainly to get realistic boundaries for available torque and power and relevant response times. Therefore, these models are not very detailed, but it is still possible to show that it is possible to get robust control in the main control loops using simple controllers.

The developed models that describes the interaction between a rigid wheel and terrain are shown to be suitable for dynamic simulations, since they need a reasonable low computational effort. The models for pneumatic tyres on soft ground are rather computationally intensive, since the equilibrium between the tyre and the terrain has to be found. Therefore, it is beneficial to perform calculations at different slips and sinkage conditions beforehand to create a map of the model, that can be utilised during the dynamic simulations in order to get reasonable low time consuming simulations. For the value of the application of the models, it is also important to consider measurement techniques to get reasonable parameter values for the models. Therefore a large part of the work was devoted to development and evaluation of such techniques. It was found that most of the parameters needed for the models were also possible to measure with a Bevameter. Still, methods to measure the point of the maximum pressure needs to be further developed.

Altogether, the developed models form a base for simulating the dynamic behaviour of a six-wheeled vehicle on both rigid and soft ground. When considering mobility, it is possible to simulate the effects of different torque distributions on the wheels, which makes it possible to develop control strategies for improved mobility in a simulated environment. Included applications of the models are: evaluating of steering strategies, improving pivot turning speed and evaluating strategies for improving at-the-limit handling and the contribution also considers models for both on- and off-road performance.

Chapter 9

Recommendations to future work

The considered vehicle with electric transmission and individual wheel torque control makes it possible to implement performance improving functions, such as optimising pivot turning as is shown in Chapter 5.4 and improving at-the-limit handling as is shown in *Paper F*. There are also opportunities to improve off-road performance by distributing torque to the wheels with best grip. At the same time, it is easy to avoid braking some wheels due to unequal rolling distances for the wheels while cornering or running on uneven ground, which often happens during those circumstances on vehicles with conventional mechanical transmission and locked differentials.

However, when running on soft, weak ground, the torque distribution becomes a delicate challenge. When driving straight forward on flat, soft ground, a vehicle with mechanical transmission usually does an excellent job, since there are only minor speed differences on the wheels due to transmission flexibility. Since weak ground easily is damaged and the vehicle might get stuck as soon as some wheel is running faster than the other wheels, the torque distribution for the electric transmission must carefully synchronise the wheel speeds in order to match the performance of the mechanical transmission. Due to communication delays between the hub motors, it might be really hard or even impossible to use torque as the command to the hub motors. A solution might be to use speed controllers in the hub motor controllers to avoid that one or more wheels would run too fast and damaging the ground. With only torque control in the hub motor controllers, it might be hard to start driving on soft ground. If the

driver is slowly increasing the wheel torques as the vehicle is standing still, one or a few wheels are likely to start rotating before the others, and the vehicle might get stuck. More functions can be added to adapt the wheel speeds while cornering and avoid braking wheels due to different rolling lengths when running on uneven ground.

To be able to evaluate strategies for running on soft, weak ground in a simulation environment, the tyre/terrain interaction models in *Paper E* have to be extended to include slip-sinkage. It is possible to decrease the drawbar pull at excessive slip for example by moving the point of maximum pressure, θ_m, forward in the tyre/terrain interface. It might be useful to include a dynamic model or at least keeping track of when excessive slip occurs, since wheels might get severely stuck due to the sinkage. To simulate cornering manoeuvres on soft ground, the model has to include lateral forces. One method to include lateral shear forces in the tyre/terrain interface is described in *Paper C*, and that method can also be applied to the model described in *Paper E*. To make the lateral forces more realistic, also lateral forces due to "bull-dozing" are possible to include.

In *Paper F* it is shown that applying rear wheel steering does not help during a rear wheel skid. Also, since the possible rear wheel steering angle on the considered vehicle is large, and due to the inherent instability of the rear wheel steering, the system is considered to be safety critical. If the rear wheel steering angle is accidentally increased, the vehicle would be hard to control and there is a risk of overturning. If the rear wheel steering is not working and the rear wheels are always locked in the aligned position, the vehicle performance is reduced since the turning diameter becomes larger, but this is normally not dangerous. Thus, the rear wheel steering system is considered a fail-safe system. One way to deal with that is to ensure that the rear wheel steering system is always locked in the aligned position when the vehicle is running fast. Since the rear wheel steering system is of no use during a rear wheel skid and the fail-safe issue makes it hard to use the rear wheel steering system at high velocities, not much effort is put into designing a rear wheel steering controller in *Paper F*. However, for a vehicle with smaller rear wheel steering angle, or a fail-safe design that allows small rear wheel steering angles at high velocities, it still may be possible to increase the vehicle performance by using rear wheel steering. For example, it might be possible to stabilise the vehicle during turning manoeuvres and also avoid getting into a rear wheel skid.

All the performance improving possibilities with individual torque control and several possible ways to steer the vehicle also means that the system should be analysed for safety, since if something goes wrong and for example the torque

is distributed in an undesired way, dangerous situations might occur. Some systems, e.g. the steering system, always needs to be available to the driver command and are considered as fail operational. Systems like the rear wheel steering system, that can improve performance when they are working, but can be put into a passive, safe state when faults occur, are considered as fail safe. Usually, fail safe systems are easier and cheaper to design and manufacture than fail operational systems. However, since the vehicle is over-actuated, it might be possible to consider the whole system and thereby simplify the architecture. For example, it might be possible to design an architecture where the steering function is fail operational, while all individual subsystems that can contribute to the steering function are fail safe. One advantage with several non-identical subsystem contributing to a safety critical function is that the probability of introducing systematic errors is reduced. Certainly, it would be necessary to analyse the different systems to ensure that the probability is sufficiently low for all subsystems to fail at the same and disabling the safety critical function.

References

[1] K. Huh, J. Kim, and J. Hong. Handling and driving characteristics for six-wheeled vehicles. *Proceedings of the Institution of Mechanical Engineers, Part D: Journal of Automobile Engineering*, 214(2):159–170, 2000.

[2] B. Chen, C. Yu, and W. Hsu. Steering control of six-wheeled vehicles using linear quadratic regulator techniques. *Proceedings of the Institution of Mechanical Engineers, Part D: Journal of Automobile Engineering*, 221(10):1231–1240, 2007.

[3] S. An, K. Yi, G. Jung, K. I. Lee, and Y. Kim. Desired yaw rate and steering control method during cornering for a six-wheeled vehicle. *International Journal of Automotive Technology*, 9(2):173–181, 2008.

[4] A. Jackson, M. Brown, D. Crolla, A. Woodhouse, and M. Parsons. Utilising the potential of individual wheel control on a 6x6 off-road vehicle. *Proceedings of ASME International Mechanical Engineering Congress and Exposition*, volume 2, pages 643–648, 2001.

[5] J. Shang, Z. Luo, D. Fan, and F. Zhao. A six wheeled robot with active self-adaptive suspension for lunar exploration. *International Technology and Innovation Conference*, pages 2035–2038, 2006.

[6] X. Yu, Y. Wang, M. Wang, and L. Wang. Obstacle-climbing capability analysis of six-wheeled rocker-bogie lunar rover on loose soil. *2nd International Conference on Intelligent Robotics and Applications*, volume 5928 LNAI, pages 1183–1189, 2009.

[7] D. Toffin, G. Reymond, A. Kemeny, and J. Droulez. Role of steering wheel feedback on driver performance: Driving simulator and modeling analysis. *Vehicle System Dynamics*, 45(4):375–388, 2007.

[8] Y. Yang, M. Parten, J. Berg, and T. Maxwell. Modeling and control of a hybrid electric vehicle. *52nd Vehicular Technology Conference*, volume 5, pages 2095–2100, September 2000.

[9] P. Caratozzolo, M. Serra, C. Ocampo, and J. Riera. A proposal for the propulsion system of a series hybrid electric vehicle. *34th Annual Power Electronics Specialists Conference*, volume 2, pages 586–591. IEEE, June 2003.

[10] S. E. Lyshevski. Diesel-electric drivetrains for hybrid-electric vehicles: New challenging problems in multivariable analysis and control. *Proceedings of the 1999 IEEE International Conference on Control Applications*, pages 840–845, August 1999.

[11] B. Ferhadbegovic, C. Brinkmann, and H. D. Kutzbach. Dynamic longitudinal model for agricultural tyres. *Proceedings of the 15th international conference of the ISTVS*, 2005.

[12] H. Pacejka. *Tyre and vehicle dynamics*. Elsevier Butterworth-Heinemann, 2002.

[13] J. Svendenius. *Tire models for use in braking applications*. Licentiate thesis, Lund Institute of Technology, Lund, Sweden, November 2003.

[14] J. Y. Wong. *Theory of ground vehicles*. John Wiley & Sons, Inc., 1978.

[15] J. Y. Wong. *Terramechanics and Off-Road Vehicles*. Elsevier Science Publishers B.V., 1989.

[16] A. Bodin. Bevameter — development of a device to characterize the characteristics of soft terrain. *Proceedings of the 8th European Conference of the ISTVS*, pages 1 – 8, 2000.

[17] J. Wong and A. Reece. Prediction of rigid wheel performance based on analysis of soil – wheel stresses – 1. *Journal of Terramechanics*, 4(1):81 – 98, 1967.

[18] Z. Janosi and B. Hanamoto. Analytical determination of draw bar pull as a function of slip for tracked vehicles in deformable soils. *Proceedings of the 1st International Conference of the International Society for Terrain-Vehicles Systems*, 1961.

[19] K. Yoshida and G. Ishigami. Steering characteristics of a rigid wheel for exploration on loose soil. *2004 IEEE/RSJ International Conference on Intelligent Robots and Systems (IROS)*, 4:3995 – 4000, 2004.

[20] W. Qiao. Study about the desert mobility of tyre with wide cross-section and low inflation pressu re. *Proceedings of the 15th international conference of the ISTVS*, Hayama, Japan, 2005.

[21] B. J. Chan and C. Sandu. A semi-analytical approach to off-road tire modeling for vehicle dynamics simulations. *Proceedings of the 16th International conference of the ISTVS*, Torino, Italy, 2008.

[22] Y. Fujimoto. Performance of elastic wheels on yielding cohesive soils. *Journal of Terramechanics*, 14(4):191 – 210, 1977.

[23] E. Wennerström, S. Nordmark, and B. Thorvald. *Fordonsdynamik*. Kungl. Tekniska Högskolan, 1999.

[24] D. R. Freitag and M. E. Smith. Center-line deflection of penumatic tires moving in dry sand. *Journal of Terramechanics*, 3(1):31 – 46, 1966.

[25] A. Bodin. Bevameter – development of a device to characterize the characteristics of soft terrain. *Journal of Terramechanics*, 38(3):47 – 59, 2001.

[26] M. G. Bekker. *Introduction to terrain-vehicle systems*. University of Michigan Press, Ann Arbor, Michigan, United States, 1969.

[27] A. R. Reece. Introduction to terrain-vehicle systems. *Proc. Institution of Mechanical Engineers*, 180(2A), 1965 – 1966.

[28] O. Noréus. Six-wheeled vehicle steering. *Proceedings of the 15th international conference of the ISTVS*, 2005.

[29] L. L. Karafiath. Plasticity theory and the stress distribution beneath wheels. *Journal of Terramechanics*, 8(2):49 – 60, 1971.

[30] K. W. Wiendieck. A theoretical evaluation of the sheer-to-normal stress ratio at the soil-wheel interface. *Journal of Terramechanics*, 5(4):9 – 25, 1968.

[31] K. W. Wiendieck. Stress-displacement relations and terrain-vehicle mechanics: A critical discussion. *Journal of Terramechanics*, 5(3):67 – 85, 1968.